



## tRNA-derived small RNAs are embedded in the gene regulatory program instructing *Drosophila* metamorphosis

Junling Shi, Jiaqi Xu, Jun Ma, et al.

*Genome Res.* published online November 16, 2023

Access the most recent version at doi:[10.1101/gr.278128.123](https://doi.org/10.1101/gr.278128.123)

---

<b>P&lt;P</b>	Published online November 16, 2023 in advance of the print journal.
<b>Accepted Manuscript</b>	Peer-reviewed and accepted for publication but not copyedited or typeset; accepted manuscript is likely to differ from the final, published version.
<b>Creative Commons License</b>	This article is distributed exclusively by Cold Spring Harbor Laboratory Press for the first six months after the full-issue publication date (see <a href="https://genome.cshlp.org/site/misc/terms.xhtml">https://genome.cshlp.org/site/misc/terms.xhtml</a> ). After six months, it is available under a Creative Commons License (Attribution-NonCommercial 4.0 International), as described at <a href="http://creativecommons.org/licenses/by-nc/4.0/">http://creativecommons.org/licenses/by-nc/4.0/</a> .
<b>Email Alerting Service</b>	Receive free email alerts when new articles cite this article - sign up in the box at the top right corner of the article or <a href="#">click here</a> .

---

---

Advance online articles have been peer reviewed and accepted for publication but have not yet appeared in the paper journal (edited, typeset versions may be posted when available prior to final publication). Advance online articles are citable and establish publication priority; they are indexed by PubMed from initial publication. Citations to Advance online articles must include the digital object identifier (DOIs) and date of initial publication.

---

To subscribe to *Genome Research* go to:  
<https://genome.cshlp.org/subscriptions>

---

Published by Cold Spring Harbor Laboratory Press

1

2

3 **tRNA-derived small RNAs are embedded in the gene regulatory network instructing**

4

***Drosophila* metamorphosis**

5

6

Junling Shi <sup>1</sup>, Jiaqi Xu <sup>1</sup>, Jun Ma <sup>1,2,3,4,\*</sup> and Feng He <sup>1,2,3,4,\*</sup>

7

<sup>1</sup>Center for Genetic Medicine, the Fourth Affiliated Hospital, Zhejiang University School of  
Medicine, Hangzhou, Zhejiang 310058, China

<sup>2</sup>Women's Hospital, Zhejiang University School of Medicine, Hangzhou, Zhejiang 310058,  
China

<sup>3</sup>Institute of Genetics, Zhejiang University International School of Medicine, Hangzhou,  
Zhejiang 310058, China

<sup>4</sup>Zhejiang Provincial Key Laboratory of Genetic and Developmental Disorder, Hangzhou,  
Zhejiang 310058, China

8

\* Corresponding authors

9

10

Correspondence to: [jun\\_ma@zju.edu.cn](mailto:jun_ma@zju.edu.cn) (J.M.) or [feng\\_he@zju.edu.cn](mailto:feng_he@zju.edu.cn) (F.H.)

11

12 **Abstract**

13       A class of noncoding RNAs, referred to as tsRNAs, is emerging with a potential to exert  
14 a new layer in gene regulation. These RNAs are breakdown products of tRNAs, either  
15 through active processing or passive cleavage or both. Since tRNAs are part of the general  
16 machinery for translation, their expression levels and activities are tightly controlled, raising  
17 the possibility that their breakdown products, tsRNAs, may provide a link between the overall  
18 translational status of a cell to specific changes in gene regulatory network. We  
19 hypothesize that *Drosophila* pupation, being a special developmental stage during which  
20 there is a global limitation of nutrients, represents a system in which such a link may readily  
21 reveal itself. We show that specific tsRNAs indeed exhibit a dynamic accumulation upon  
22 entering the pupal stage. We describe experiments to characterize the mode of tsRNA action  
23 and, through the use of such gained knowledge, conduct a genome-wide analysis to assess the  
24 functions of dynamically expressed tsRNAs. Our results show that the predicted target  
25 genes are highly enriched in biological processes specific to this stage of development  
26 including metamorphosis. We further show that tsRNA action is required for successful  
27 pupation, providing direct support to the hypothesis that tsRNAs accumulated during this  
28 stage are critical to the gene expression program at this stage of development.

29

30 **Keywords:** tRNA-derived small RNAs, gene expression regulation, metamorphosis,  
31 *Drosophila*

## 32 **Introduction**

33 tRNA-derived small RNAs (tsRNAs, also known as tRNA-derived fragments) are among  
34 the most ancient and conserved RNA species across all organisms. Accumulating evidence  
35 suggests that, from bacteria to human, tsRNAs are not merely intermediates of the tRNA  
36 maturation process or residues of the tRNA degradation process as their biogenesis can  
37 exhibit elaborate spatiotemporal patterns (Kumar et al. 2016; Sharma et al. 2016; Li et al.  
38 2018; Dou et al. 2019; Chen et al. 2021b; Krishna et al. 2021). tsRNAs have a relatively  
39 wide range of size and abundant modifications, with a potential to interact with a variety of  
40 biomolecules to exert diverse functions (Haussecker et al. 2010; Schaefer et al. 2010; Tuorto  
41 et al. 2012; Hussain et al. 2013; Kumar et al. 2014; Guzzi et al. 2018; Luo et al. 2018).  
42 tsRNAs with a length of 20~24 nt can participate in posttranscriptional regulation through  
43 mRNA hybridization and Argonaute (AGO) engagement. In this way that resembles RNA  
44 interference (RNAi), tsRNAs could suppress the stability or translation of target mRNAs.  
45 For example, in mature B lymphocytes, a 3' fragment derived from tRNA<sup>GlyGCC</sup> (referred to as  
46 3'-tsRNA<sup>GlyGCC</sup>) has activities characteristic of a miRNA, including the capacity of binding to  
47 all four human AGOs and gene silencing via target sites in 3' UTRs (Maute et al. 2013). In  
48 addition, tsRNAs can associate with RNA-binding proteins other than AGOs in a cell type  
49 and status-specific manner. In breast cancer cells, four tsRNA species encompassing the  
50 anticodon loops (referred to as inter-tsRNA<sup>GluYUC</sup>, tsRNA<sup>AspGUC</sup>, tsRNA<sup>GlyUCC</sup> and  
51 tsRNA<sup>TyrGUA</sup>) have been reported to compete against oncogenic mRNAs for binding with  
52 YBX1 and suppress their stability (Goodarzi et al. 2015). Moreover, tsRNAs can frequently  
53 associate with translation machinery and related factors to participate in multiple layers of

54 translation control, such as rRNA biogenesis, ribosome assembly, translation initiation and  
55 translation elongation (Couvillion et al. 2010; Ivanov et al. 2011; Couvillion et al. 2012;  
56 Gebetsberger et al. 2012; Sobala and Hutvagner 2013; Gebetsberger et al. 2017; Keam et al.  
57 2017; Kim et al. 2017). Finally, tsRNAs have been reported to bind to gene promoter  
58 regions to induce transcriptional reprogramming during early embryonic development of  
59 mouse and zebrafish (Chen et al. 2016; Chen et al. 2021a). These diverse and  
60 context-dependent functions of tsRNAs suggest a need for a comprehensive profiling and  
61 functional analysis of tsRNAs at the systems level within a developmental context.

62

63       Development is a process where cells can adaptively respond to environmental  
64 fluctuations by rewiring gene regulatory networks. In particular, suppression on protein  
65 synthesis usually provides cells with a resource allocating solution within a few minutes of  
66 exposure to stress (Lopez-Maury et al. 2008). As a class of key informational molecules in  
67 the process of translation, tRNAs may contribute to such a solution through non-canonical  
68 functions that are mediated by other forms, such as tsRNAs. Previous studies in cell cultures  
69 have shown that nutrient deprivation can cause tRNAs to break down resulting in an  
70 accumulation of tsRNAs and down-regulation of translation (Lee and Collins 2005;  
71 Haussecker et al. 2010; Sobala and Hutvagner 2013; Luo et al. 2018). It remains unclear if  
72 such a scenario, or a varied version of it, could play out in a developmental context to  
73 contribute to the successful progression of developmental programs. Here we selected  
74 metamorphosis in *Drosophila* as a developmental window to probe this question aimed at  
75 gaining a systematic view of tsRNA action. Metamorphosis of insects is an intricate and

76 deterministic developmental process. As larvae stop feeding to transition into the pupal  
77 stage, the nutritional input is cut off, forcing the animals to rely on the energy store  
78 accumulated by larvae to perform large-scale remodeling and complete the larva-to-adult  
79 transition (Merkey et al. 2011; Rolff et al. 2019; Li et al. 2022). A signature of the  
80 larva-to-pupa transition is a global decline in translation accompanied by a reduction in  
81 translation efficiency for proteins in the translation machinery itself (see Results), providing  
82 an excellent developmental system for a systematic analysis of tsRNA functions.  
83

## 84 **Results**

### 85 **A quantitative RNA-seq approach for analyzing tsRNAs during larva-to-pupa transition**

86 We employed mim-tRNAseq (modification-induced misincorporation tRNA sequencing),  
87 an RNA-seq pipeline designed for tRNA analysis (Behrens et al. 2021), in our study of  
88 tsRNAs in *Drosophila melanogaster*. The library construction step of this pipeline includes  
89 necessary measures to minimize tRNA modifications that can hinder effective detection and  
90 quantitation in deep sequencing. In our experiments, we used size selection optimized  
91 specifically for detecting tsRNAs and tRNAs and adopted a ‘paired’ library construction  
92 approach to permit direct comparisons between tRNA and tsRNA data for each RNA sample  
93 (Figure 1A; Materials and Methods). We focused on three developmental stages spanning  
94 the larva-to-pupa transition in our study: third instar larvae, first- and second-day pupae (L3,  
95 P1 and P2, respectively).

96  
97 To evaluate the performance of mim-tRNAseq under our experimental setup, we  
98 analyzed different quantitative aspects of our data. Over 95% of the alignments with the  
99 genomic tRNA reference in our both tRNA and tsRNA datasets are unambiguous (see  
100 Supplemental Table S1 for library information and mapping statistics). A nearly uniform  
101 pattern of read coverage along the length of nuclear genome-encoded tRNA with a modest  
102 weakening toward the 5’ end (Supplemental Fig. S1A) is generally consistent with published  
103 results (Behrens et al. 2021). In addition, the expression level of tRNAs exhibited a general  
104 correlation with the copy numbers of their corresponding genes (Pearson’s correlation  $\rho \approx 0.6$   
105 and  $p < 10^{-4}$  for all our datasets; Supplemental Fig. S1B). In particular, within each pair of

106 isoacceptor tRNAs ( $\text{tRNA}^{\text{GlyGCC}}/\text{tRNA}^{\text{GlyUCC}}$ ,  $\text{tRNA}^{\text{GluCUC}}/\text{tRNA}^{\text{GluUUC}}$  and  
107  $\text{tRNA}^{\text{LysCUU}}/\text{tRNA}^{\text{LysUUU}}$ ), the relative difference in tRNA expression was also consistent with  
108 the difference in gene copy number (Supplemental Fig. S1C), suggesting single-nucleotide  
109 resolution of our datasets. The tRNA abundances (RPM, reads per million) displayed an  
110 excellent reproducibility between biological replicates and a relative stability from L3 to P2  
111 (Figure 1B). The overall stability of tRNA abundances during the larva-to-pupa transition  
112 was further supported by three additional analyses (Supplemental Fig. S1D-F): 1) absolute  
113 quantification of total tRNA concentration using a spike-in control (*E. coli*  $\text{tRNA}^{\text{LysUUU}}$ ); 2)  
114 quantification of total tRNAs using SYBR Gold staining; 3) Northern blots against selected  
115 tRNAs ( $\text{tRNA}^{\text{AspGUC}}$ ,  $\text{tRNA}^{\text{GlyGCC}}$  and  $\text{tRNA}^{\text{GluCUC}}$ ). Together, these results document a  
116 suitability of the mim-tRNAseq pipeline in efficiently and accurately detecting tRNAs under  
117 our experimental setup.

118

119 To evaluate the feasibility of using the mim-tRNAseq pipeline to profile the dynamic  
120 expression of tsRNAs in our datasets, we generated tsRNA data (Figure 1C) that were paired  
121 with the tRNA data (Figure 1B). Figure 1D shows that, when grouped according to the  
122 anticodon, the tsRNA abundances exhibited significant correlations with the tRNA gene copy  
123 numbers, the tRNA abundances, the tsRNA abundances measured by PANDORA-seq  
124 (panoramic RNA display by overcoming RNA modification aborted sequencing)(Shi et al.  
125 2021), and the tsRNA abundances obtained from published small RNA libraries (Pearson's  
126 correlation  $\rho = 0.65\sim 0.82$  and  $p < 10^{-5}$ ; see Supplemental Fig. S2 for comparisons of  
127 individual libraries). Furthermore, the changes of tsRNA abundances between different

128 developmental stages revealed by our sequencing data were verified through the use of three  
129 high-abundance 5'-tsRNAs in Northern blot analysis (see below and Figure 2H for details).  
130 Together, these results supported a feasibility of using the mim-tRNAseq pipeline for  
131 quantitatively analyzing tsRNA data in our experimental setup. We referred to our adopted  
132 pipeline as mim-tRNA/tsRNA-seq.

133

### 134 **Accumulation of 5'-tsRNAs during larva-to-pupa transition**

135 According to our mim-tRNA/tsRNA-seq data, the size distribution of tsRNAs exhibited a  
136 sharper peak at ~34 nt in early pupae than in larvae, with this peak (30~35 nt) accounting for  
137 45.7%, 72.7% and 71.2% of total tsRNAs in L3, P1 and P2, respectively (Figure 2A). This  
138 could be explained by an active event of tRNAs being processed into tRNA halves during the  
139 larva-to-pupa transition. To infer this process, we calculated the relative coverage of tsRNA  
140 reads at each nucleotide position on the corresponding tRNAs in the three developmental  
141 stages. Figure 2B shows an uneven overall distribution of tsRNAs along the tRNA length,  
142 with a higher abundance in 5'-half than 3'-half for most tRNAs. A clear demarcation was  
143 detected near the middle of tRNAs separating the two halves, suggesting an overall  
144 preference of cleavage at the anticodon loop over D-loop or T-loop. This demarcation  
145 appeared sharper toward 5'-half than 3'-half, suggesting a relatively more subdued  
146 post-cleavage processing for 5'-tsRNAs compared with 3'-tsRNAs. No such boundary was  
147 obvious at the position expected of T-loop cleavage, suggesting that further processing of  
148 3'-tsRNAs was not a result of endonuclease cleavage at the T-loop.

149

150 The uneven distribution of tsRNA sequencing reads between 5' and 3'-halves was  
151 independent of the developmental stages analyzed (Figure 2B; see also Supplemental Fig.  
152 S3A for a similar pattern of PANDORA-seq data), suggesting an overall mechanistically  
153 similar pattern of cleavage within the anticodon loops at these stages. However, 5'-tsRNAs  
154 exhibited more degenerated 3' ends in L3 than those in P1 and P2 (Figure 2B arrows),  
155 suggestive of de novo tRNA processing during the larva-to-pupa transition. To directly  
156 measure the change of tsRNA levels across different stages, we performed quantification by  
157 normalizing the tRNA-mapped reads to 2S rRNA (RPKR, reads per kilo 2S rRNA-mapped  
158 reads; see Supplemental Fig. S4A for Northern blot against 2S rRNA documenting its stable  
159 expression during these stages) or to the *E. coli* spike-in (RPKE, reads per kilo *E. coli*  
160 tRNA-mapped reads). We observed a good correlation between the biological replicates of  
161 each developmental stage, indicating high reproducibility (Supplemental Fig. S4B). Both  
162 approaches supported a significant increase of total tsRNAs in P1 and P2 relative to L3,  
163 suggesting an overall accumulation of tsRNAs during the larva-to-pupa transition (Figure 2C).  
164 Given the developmental stability of tRNA abundances, tsRNA accumulation also manifested  
165 itself as an increased slope of tsRNA abundance against their paired tRNA abundance  
166 (log-log slopes = 0.308, 0.416 and 0.604 arbitrary unit for L3, P1 and P2, respectively; Figure  
167 2D). Our results are in agreement with limited available findings reported previously (Luo  
168 et al. 2018) and, together, they documented an active accumulation of tsRNAs during the  
169 larva-to-pupa transition.

170

171       Based on tsRNA length and location in their corresponding tRNAs, we further grouped  
172 tsRNAs into five subclasses as described in (Su et al. 2020): 5-tRFs, 5-tRHs, Inter-tRFs,  
173 3-tRHs and 3-tRFs (Figure 2E top, see also Supplemental Fig. S3B for PANDORA-seq data).  
174 We observed overall good correlations between tsRNAs in each of these subclasses and the  
175 corresponding tRNAs at each developmental stage, supportive of post-transcriptional  
176 biogenesis of all these tsRNAs (Supplemental Fig. S5A). We found that Inter-tsRNAs had  
177 the lowest overall levels (measured as RPKR) in all three stages (Figure 2E middle), further  
178 supporting a preference of tRNA cleavage at the anticodon loop. The overall accumulation  
179 in the pupal stages of 5-tRHs appeared slightly more robust than that of 3-tRHs (Figure 2F),  
180 as further evidenced by a direct comparison of fold increases after pupation between these  
181 two tsRNA subclasses (Kolmogorov–Smirnov test  $p < 0.0001$ ; Figure 2G). Such  
182 asymmetric pattern of accumulation suggests an increased post-cleavage stability of 5-tRHs  
183 relative to 3-tRHs. Together these results suggested a prominent contribution of 5'-tsRNAs,  
184 in particular 5-tRHs, to the overall increase in tsRNA levels during the larva-to-pupa  
185 transition.

186

187       To further confirm such an accumulation, we performed Northern blot analyses on  
188 selected 5'-tsRNAs. Here we chose three with relatively high abundances: 5'-tsRNA<sup>Asp<sup>GUC</sup></sup>  
189 (RPKR = 52.9, 797.7 and 363.5 in L3, P1 and P2, respectively), 5'-tsRNA<sup>Gly<sup>GCC</sup></sup> (RPKR =  
190 98.8, 755.2 and 484.2) and 5'-tsRNA<sup>Glu<sup>CUC</sup></sup> (RPKR = 36.4, 249.7 and 123.4). We found that,  
191 while 5S rRNA and the corresponding tRNAs exhibited relatively stable levels of expression  
192 from L3 to P2, the selected 5'-tsRNAs all showed a clear increase after pupation (Figure 2H).

193 In fact, the expression of all the selected 5'-tsRNAs peaked in early pupae throughout the  
194 entire life cycle of *Drosophila melanogaster* (Supplemental Fig. S5B). In contrast,  
195 3'-tsRNA<sup>AspGUC</sup> (RPKR = 16.1, 85.6 and 60.2) was verified to have a consistently lower level  
196 of expression (Supplemental Fig. S5C). We also confirmed such an accumulation of  
197 selected 5'-tsRNAs in *Drosophila simulans* and *Drosophila yakuba* (Supplemental Fig. S5D).  
198 Altogether, these results suggested that 5'-tsRNAs accumulation during the larva-to-pupa  
199 transition in *Drosophila* is a developmentally-controlled and evolutionarily-conserved event.

200

### 201 **5'-tsRNAs exert regulatory activities through target site recognition on mRNAs**

202 To analyze the regulatory activities of tsRNAs during pupation, we performed tsRNA  
203 inhibition experiments *in vivo* using the 'sponge' methodology. Here we expressed a  
204 silencing cassette with 10 repetitive sequences that are complementary to a 5'-tsRNA to be  
205 inhibited (Figure 3A and Supplemental Table S2). This method follows Watson-Crick base  
206 pair complementarity, a method that has been successfully used in elucidating miRNA  
207 functions in a variety of species, both *in vivo* and *in vitro* (Ebert et al. 2007; Ebert and Sharp  
208 2010a; Fulga et al. 2015). Five tsRNAs were selected for sponge analysis: 5'-tsRNA<sup>AspGUC</sup>,  
209 5'-tsRNA<sup>GlyGCC</sup>, 5'-tsRNA<sup>GluCUC</sup>, 5'-tsRNA<sup>ProUGG</sup> and 5'-tsRNA<sup>LysUUU</sup>. Among them,  
210 5'-tsRNA<sup>AspGUC</sup>, 5'-tsRNA<sup>GlyGCC</sup>, 5'-tsRNA<sup>GluCUC</sup> and 5'-tsRNA<sup>ProUGG</sup> were selected because  
211 their high abundances in early pupal stages according to our mim-tRNA/tsRNA-seq and  
212 PANDORA-seq data (Figures 2E and S3B). 5'-tsRNA<sup>LysUUU</sup> was shown to be strongly  
213 induced under serum starvation in *Drosophila* S2 cells (Luo et al. 2018). Furthermore, we

214 generated a sponge line against a sequence scrambled from 5'-tsRNA<sup>AspGUC</sup> (Supplemental  
215 Table S2), which represents a negative control in addition to no sponge (see below).

216

217 To maximize the detection of changes in gene expression upon tsRNA inhibition, we  
218 used a ubiquitous driver, *Tubulin-GAL4*, to express each of the sponges and performed  
219 transcriptomic analyses in early pupae. For 5'-tsRNA<sup>GlyGCC</sup>, 5'-tsRNA<sup>GluCUC</sup>,  
220 5'-tsRNA<sup>ProUGG</sup> and 5'-tsRNA<sup>LysUUU</sup>, the samples were collected in P2; for 5'-tsRNA<sup>AspGUC</sup>,  
221 the samples were collected in P1 (due to lethality prior to P2; see Figure 5B-C). To exclude  
222 the possibility that our sponges may affect tRNA levels or functions in either direct or indirect  
223 manners, we performed Northern blot and qRT-PCR experiments. The quantification results  
224 showed that the expression levels of full-length tRNAs stayed mostly unaltered in  
225 *Tubulin-GAL4>2*×sponge pupae (Supplemental Fig. S6A-B). In addition, by comparing the  
226 5'-tsRNA<sup>AspGUC</sup> sponge line and its scramble control, our mRNA/Ribo-seq analysis did not  
227 detect a significant difference in either single-codon ribosome occupancies or translation  
228 efficiency (TE; see Materials and Methods) of genes enriched with codons GAC/U  
229 (Supplemental Fig. S6C-D). Furthermore, our PANDORA-seq analysis of the  
230 5'-tsRNA<sup>AspGUC</sup> sponge and its scramble control demonstrated that the levels of most of the  
231 detectable miRNAs and piRNAs were not significantly different (Supplemental Fig. S6E).

232

233 We used DESeq2 to conduct a two-factor analysis, accounting for both developmental  
234 stages (P1 vs. P2) and genotypes (*Tubulin-GAL4>2*×sponge vs. no sponge). By contrasting  
235 the genotypes, we identified differentially expressed genes (DEGs) and performed Gene

236 Ontology (GO) annotation. A total of 438 genes were identified with significantly lower  
237 mRNA expression ( $\log_2(\text{fold change}) < -1$  and adjusted  $p < 0.05$ ) in the five  
238 *Tubulin-GAL4>2*×sponge lines, but without a significant clustering in any functional category.  
239 On the contrary, a total of 1,097 genes with significantly higher mRNA expression in the  
240 sponge lines were enriched in a few key pathways for pupal development such as ‘response to  
241 biotic stimulus’ and ‘cuticle development’ (adjusted  $p = 10^{-7}$  and  $10^{-14}$ , respectively; Figure  
242 3B). Therefore, the pupa-accumulated 5'-tsRNA in our test could suppress specific gene  
243 activities that are crucial for pupal development.

244

245 The actions of tsRNAs on gene expression could depend on their recognition sites in  
246 targeted mRNAs (Maute et al. 2013; Luo et al. 2018). We combined three algorithms,  
247 TargetScan, phyloP and miRanda, to predict mRNA target sites that could fulfill the  
248 following three criteria: 1) at least 7-bp perfect antisense match to the tsRNA sequence; 2)  
249 FDR-adjusted cross-species conservation score for the mRNA site  $< 0.05$ ; 3) a minimum free  
250 energy (MFE)  $< -30$  kCal/mol of local alignment. Based on the number of predicted target  
251 sites on each mRNA, we classified the expressed genes into four groups for each tsRNA  
252 sponge that we analyzed: no sites, 1~2 sites, 3~4 sites and  $\geq 5$  sites. Figure 3C shows an  
253 mRNA level increase in response to the sponges against 5'-tsRNA<sup>Asp<sup>GUC</sup></sup>, 5'-tsRNA<sup>Gly<sup>GCC</sup></sup>,  
254 5'-tsRNA<sup>Glu<sup>CUC</sup></sup> and 5'-tsRNA<sup>Pro<sup>UGG</sup></sup> in a manner that is dependent on the number of predicted  
255 target sites. In contrast, when 5'-tsRNA<sup>Lys<sup>UUU</sup></sup> was sponged, the mRNA levels of genes with  
256 or without putative target sites effectively had no difference (Figure 3D). This tsRNA had  
257 the lowest abundance (RPKR = 89.6 in P2) among the tsRNAs tested, suggesting that the

258 inhibitory effect detected in our sponge setup is dependent on tsRNA abundance. To further  
259 evaluate this point, we found that our data obtained with sponges against 5'-tsRNA<sup>GlyGCC</sup>,  
260 5'-tsRNA<sup>GluCUC</sup> and 5'-tsRNA<sup>ProUGG</sup> each yielded similar results when either 5'-tsRNA<sup>LysUUU</sup>  
261 sponge or no sponge was used a negative control (Supplemental Fig. S7A). Furthermore, we  
262 found that the scramble sponge had no meaningful effect on mRNA levels irrespective of the  
263 number of 'target' sites (Figure 3E). In addition, our data obtained with the sponge against  
264 5'-tsRNA<sup>AspGUC</sup> at P1 yielded similar results when either this scramble sponge or no sponge  
265 was used as a negative control (Supplemental Fig. S7B).

266

267 **Effective mRNA-level inhibition has no strict requirements of either mRNA site location**  
268 **or tsRNA seed selection**

269 To investigate whether tsRNAs may exhibit a preference in target site location on mRNA,  
270 we selected genes containing predicted target sites in only one section of their transcripts and  
271 divided them into three classes based on target site positions on the transcript: 5' UTR, CDS  
272 and 3' UTR. Supplemental Fig. S7C shows that, among the 5'-tsRNAs analyzed,  
273 5'-tsRNA<sup>AspGUC</sup> had a significant preference of target site location in CDS and 5' UTR over 3'  
274 UTR. However, 5'-tsRNA<sup>GlyGCC</sup>, 5'-tsRNA<sup>GluCUC</sup> and 5'-tsRNA<sup>ProUGG</sup> did not exhibit such a  
275 preference, with varying degrees of inhibition when they were at different locations. These  
276 results suggested that the inhibitory effect exerted by tsRNAs through their presumed target  
277 genes is largely independent of tsRNA target site location on the transcript.

278

279 It is well documented that miRNA action mainly depends on the ‘seed’ positioned at the  
280 nucleotide 2~8 at the 5’ end. To evaluate whether the mode of tsRNA action may share this  
281 feature, we analyzed the inhibitory effect of each 7-mer seed from 5’ to 3’ along  
282 5’-tsRNA<sup>GlyGCC</sup>, 5’-tsRNA<sup>GluCUC</sup>, 5’-tsRNA<sup>ProUGG</sup> and 5’-tsRNA<sup>AspGUC</sup>. While the seeds at  
283 varied positions of 5’-tsRNAs did not exhibit a gross bias in their ability to affect their  
284 presumed target mRNA levels, the majority of them showed clear de-repression on target  
285 genes by the corresponding tsRNA sponge (Supplemental Fig. S7D). These results  
286 suggested that 5’-tsRNA recognition of their target sites was not restricted to the 5’ seed  
287 selection as seen for miRNAs.

288

### 289 **Participation of accumulated tsRNAs in regulating the expression of metamorphosis** 290 **genes**

291 Our results described thus far suggested that tsRNAs could repress mRNA expression of  
292 target genes with an accommodating posture in terms of both seed selection and site location.  
293 Based on this mode of tsRNA action, we performed a genome-wide analysis to determine  
294 whether dynamically expressed tsRNAs may target genes that are relevant to developmental  
295 processes at early pupal stages. Here we analyzed tsRNAs that were expressed in P2 and  
296 compiled all mim-tsRNA-seq reads according to the functional unit of 7-mer seeds. This led  
297 to the identification of 2,075 unique seeds. We selected the top 5% of these seeds with the  
298 highest abundance. At this abundance threshold, 104 seeds were captured, which  
299 contributed to 42% of the total tsRNA reads in P2 and had an increased RPKR by at least 2.1  
300 fold in P2 than in L3 (Student’s *t*-test *p*-value < 0.0001). Among them, only one was shared

301 by known miRNA families: “GUAGAAU” as in miR-958, which was found to be adult  
302 gut-specific (Weigelt et al. 2019).

303

304 We used the 104 seeds to scan the genome for recognition sites (Materials and Methods).  
305 We calculated the density of these sites in the transcript of each protein-coding gene, and  
306 retrieved a total of 1,418 genes with the top site density (9.1~55.8 sites per kb) and a  
307 detectable level of mRNA expression (DESeq2-calculated baseMean > 70). We considered  
308 them as putative target genes of highly-expressed tsRNAs at P2 stage (also significantly  
309 up-regulated from L3 to P2 with fold change > 2.1 and Student’s *t*-test *p*-value < 0.0001) for  
310 further analyses. GO annotation revealed that these genes were significantly enriched in  
311 essential biological processes including ‘metamorphosis’ and ‘cytoplasmic translation’  
312 (Figure 4A). Since this genome-wide screening was performed without a precondition of  
313 gene expression status, our results suggested that the accumulated tsRNAs at early pupal  
314 stages have a preference for targeting genes including those that are involved in biological  
315 processes taking place at this time.

316

317 To examine whether the accumulated tsRNAs in early pupae exert regulatory activities  
318 on their putative target genes during normal development, we analyzed our mRNA-seq data  
319 of WT across different stages. Enriched GO groups of genes with an increased mRNA level  
320 include “mitochondrion organization” (GO:0007005), “cuticle development” (GO:0042335)  
321 and “protein targeting” (GO:0006605); those with a decreased level include “mitotic cell  
322 cycle” (GO:0000278), “metamorphosis” (GO:0007552), “lipid homeostasis” (GO:0055088),

323 “alpha-amino acid metabolic process” (GO:1901605) and “proteolysis involved in cellular  
324 protein catabolic process” (GO:0051603). These results are in general agreement with  
325 existing knowledge (Zhang et al. 2020) about the developmental events during the  
326 larva-to-pupa transition. Figure 4B shows that the putative target genes had a significant  
327 overall reduction in mRNA levels (between P2 and L3). When these putative target genes  
328 were categorized according to GO annotation as: ‘metamorphosis’, ‘cytoplasmic translation’  
329 and ‘others’, they behaved differently from one another. Among the three groups, the  
330 ‘metamorphosis’ group of tsRNA target genes exhibited the largest reduction (Figure 4C red).  
331 This effect was also observed for the ‘others’ group but only in a modest manner (Figure 4C  
332 blue), but not for those in the ‘translation’ group (Figure 4C green). In addition, a  
333 time-series profile analysis of the 6,713 DEGs either between L3 and P1 or between P1 and  
334 P2 suggested that while the ‘metamorphosis’ group of target genes was significantly enriched  
335 in the P2-downward cluster (Figure 4D red), the ‘translation’ group was significantly enriched  
336 in the P2-upward cluster (Figure 4D green). We also examined specifically the changes of  
337 metamorphosis-associated gene product levels in response to the *Tubulin*-GAL4-driven  
338 sponges. Supplemental Fig. S8 shows that, mRNA levels of targets genes in the  
339 ‘metamorphosis’ group were significantly higher than those of their non-target counterparts  
340 (comparing red with green; Student’s *t*-test  $p < 0.001$ ) in 5’-tsRNA<sup>GlyGCC</sup>, 5’-tsRNA<sup>GluCUC</sup> and  
341 5’-tsRNA<sup>AspGUC</sup> sponge lines, respectively. Together, these results suggested a preferential  
342 impact of the accumulated tsRNAs at P2 stage on suppressing genes involved in  
343 metamorphosis.

344

## 345 **Experimental evaluation of tsRNA action and specificity**

346 Our genome-wide, informatics-based analysis described thus far suggested a  
347 participation of pupa-enriched tsRNAs in regulating the mRNA levels of  
348 metamorphosis-related genes. To further evaluate tsRNA action and specificity, we  
349 performed gene-based analyses in both S2 cells and transgenic flies. Here we manipulated  
350 tsRNA activities through the uses of tsRNA sponges, tsRNA mimics and pre-tRNA  
351 expression. In S2 cells, the expression of pre-tRNAs could moderately increase the  
352 intracellular levels of corresponding 5'-tsRNAs (see Supplemental Fig. S9A for Northern blot  
353 analysis of pre-tRNA<sup>Asp<sup>GUC</sup></sup> expression as an example). Thus, we co-transfected a synthetic  
354 tsRNA mimic (Supplemental Table S3) and an expression vector of the corresponding  
355 pre-tRNA (Supplemental Table S4) to achieve overexpression. To examine whether the  
356 inhibitory effect of 5'-tsRNAs was dependent on specific target sites, we performed  
357 dual-luciferase reporter assays by inserting three native target sites (see Supplemental Table  
358 S5 and Supplemental Fig. S9B for sequences and local alignments, respectively) of each  
359 tested 5'-tsRNA into 3' UTR or CDS of the *Renilla* gene. Figure 5A shows that the reporter  
360 activity was significantly reduced by overexpression of 5'-tsRNA<sup>Gly<sup>GCC</sup></sup>, 5'-tsRNA<sup>Glu<sup>CUC</sup></sup>,  
361 5'-tsRNA<sup>Pro<sup>UGG</sup></sup> and 5'-tsRNA<sup>Asp<sup>GUC</sup></sup> (blue), and that such an effect was blocked by their  
362 corresponding sponges (green) but not by the scramble sponge (pink). If the inserted sites  
363 were scrambled within the 7-mer seed match, tsRNA overexpression could not effectively  
364 repress the reporter activity (Figure 5A purple). In addition, we performed qRT-PCR in this  
365 system and confirmed similar results at the *Renilla* mRNA level (Supplemental Fig. S9C).

366 These results document inhibitory activities of the predicted 5'-tsRNA target sites in a  
367 cell-based reporter system.

368

369 We also used our transgenic flies containing the sponge elements to evaluate the  
370 functional consequence and action specificity of 5'-tsRNAs in a developmental context.  
371 Driven by *Tubulin*-GAL4, two of the five sponges (5'-tsRNA<sup>AspGUC</sup> and 5'-tsRNA<sup>ProUGG</sup>)  
372 exhibited pupal lethality when present at two copies (Figures 5B). The pupal lethality  
373 phenotype caused by 5'-tsRNA<sup>AspGUC</sup> sponge was significantly rescued by a simultaneous  
374 expression of pre-tRNA<sup>AspGUC</sup> (Figure 5C-D). This is a specific phenotypic rescue since it  
375 had no impact on improving the phenotype caused by another sponge against 5'-tsRNA<sup>ProUGG</sup>.  
376 In particular, ~90% pupae of *Tubulin*-GAL4>2×5'-tsRNA<sup>ProUGG</sup>-sponge were found to be  
377 insufficiently above the food surface and ~32.4% pupae failed to eclose with varied defects.  
378 These traits could not be ameliorated by the expression of pre-tRNA<sup>AspGUC</sup> (Figure 5B).

379

380 Furthermore, the observed phenotypic rescue by pre-tRNA<sup>AspGUC</sup> was accompanied by  
381 changes at in mRNA levels of selected target genes. *Arc1* encodes a retrovirus-like Gag  
382 protein that is required for regulation of neuronal synaptic plasticity, muscle development and  
383 energy balance (Mosher et al. 2015; Ashley et al. 2018). According to our prediction, *Arc1*  
384 transcript carries 4 conserved target sites of 5'-tsRNA<sup>AspGUC</sup>. qRT-PCR results showed that  
385 its mRNA level in P1 pupae of the *Tubulin*-GAL4-driven 5'-tsRNA<sup>AspGUC</sup> sponge was ~8 fold  
386 higher than that in the scramble control, and such increase was effectively restored by one  
387 copy of UAS-pre-tRNA<sup>AspGUC</sup> (Figure 5E). In fact, the *Tubulin*-GAL4-driven

388 5'-tsRNA<sup>AspGUC</sup> sponge had locomotion defects during the wondering stage (Movie S1 in  
389 compassion to the scramble control shown in Movie S2). *FASN1* and *FASN2* encode the  
390 two major fatty acid synthases in *Drosophila* (Chung et al. 2014; Garrido et al. 2015;  
391 Gramates et al. 2022). Fatty acids profiling (C14-C30) showed that heptadecanoic (17:0),  
392 stearic (18:0) and triacontanoic (30:0) acids were the most increased in 5'-tsRNA<sup>AspGUC</sup>  
393 sponge pupae (Supplemental Fig. S10A). qRT-PCR confirmed the rescue effect of  
394 pre-tRNA<sup>AspGUC</sup> on the mRNA levels of *Arc1*, *FASN1* and *FASN2* (Figure 5E). mRNA-seq  
395 further confirmed that pre-tRNA<sup>AspGUC</sup> could restore the altered mRNA levels of  
396 5'-tsRNA<sup>AspGUC</sup> target genes by 5'-tsRNA<sup>AspGUC</sup> sponge (Kolmogorov–Smirnov test  $p = 10^{-11}$ ;  
397 Figure 5F). Together, these results documented the specificity of 5'-tsRNA<sup>AspGUC</sup> action on  
398 mRNA expression of predicted target genes in a developmental context.

399

400 We also used several other GAL4 lines to drive the 5'-tsRNA<sup>AspGUC</sup> sponge (listed in  
401 Materials and Methods). The ubiquitous *Actin-GAL4*>2×sponge exhibited a similar pupal  
402 lethality phenotype with those driven by *Tubulin-GAL4*. Other tissue-specific drivers  
403 exhibited no obvious defects, except the oenocyte-specific *Desat1-GAL4* (also known as  
404 *PromE-GAL4*). All *Desat1-GAL4*>1×sponge pupae (N = 214) died before eclosion  
405 (Supplemental Fig. S10B). They showed misallocated bubbles in ventral abdomen at P2 and  
406 leg malformation at P4 (Supplemental Fig. S10C). 1×pre-tRNA<sup>AspGUC</sup> rescued the  
407 abdominal trait in all P2 pupae (N = 9; Supplemental Fig. S10C), and 3 out of 9 successfully  
408 emerged but died within the first day. Given the fact of oenocyte-specific role of *FASN2*  
409 during pupation (Billeter et al. 2009), we performed qRT-PCR and showed that, when driven

410 by *Desat1*-GAL4, 1×5'-tsRNA<sup>Asp<sup>GUC</sup></sup>-sponge elevated the mRNA level of *FASN2*, and such  
411 effect was restored by 1×pre-tRNA<sup>Asp<sup>GUC</sup></sup> (Supplemental Fig. S10D). In addition, we used  
412 RiboTag (RPL13A-FLAG) to profile oenocytes-specific ribosome-associated mRNAs in the  
413 sponge pupae, and confirmed the increase of *FASN2* expression (Supplemental Fig. S10E).  
414 These results further document that 5'-tsRNA<sup>Asp<sup>GUC</sup></sup> could act on specific target genes to  
415 achieve tissue-specific regulation during development.

416

417 **tsRNAs contribute to the regulation of an overall decline in translation efficiency during**  
418 **the larva-to-pupa transition**

419 Previous studies in S2 cells suggested that tsRNAs contribute to serum  
420 starvation-induced reduction in global translation through preferentially down-regulating  
421 translation efficiency of translational machinery genes (Luo et al. 2018). As shown by  
422 polyribosome profiling (Figure 6A), pupation is also accompanied by a decline in the overall  
423 translation. To investigate whether tsRNAs may be involved in such translation regulation  
424 with a developmental context, we performed Ribo-seq for estimating gene-specific translation  
425 efficiency (TE). As detailed above for our analysis in Figure 4C, we similarly divided the  
426 predicted target genes of pupa-accumulated tsRNAs into three functional groups  
427 (metamorphosis, translation and others). Figure 6B shows that, relative to the non-target  
428 group, target genes in the translation group had significantly down-regulated TE during the  
429 larva-to-pupa transition, contrasting with an up-regulation in TE for genes in the  
430 metamorphosis group. Clustering of time-series TE profile from L3 to P2 further supported  
431 a discrepancy in the dynamic expression pattern between the two groups of tsRNA target

432 genes (Figure 6C). As shown in Figure 4C, genes in the translation group did not have a  
433 reduced mRNA expression level in P2. Therefore, tsRNAs accumulated in early pupae can  
434 operate through a distinct, translation-mediated mechanism in regulating the overall  
435 translation efficiency during pupation.

436

## 437 **Discussion**

438 This study is designed to advance our understanding of tsRNAs function in a  
439 developmental context in *Drosophila*. It focuses on a developmental transition from an  
440 active growth and feeding state of larvae to a non-feeding and starved state of pupae in  
441 preparation of metamorphosis (Figure 6D). This transition is marked with a decline in ATP  
442 level (Yamada et al. 2020), overall translation (Figure 6A) and an accumulation of tsRNAs  
443 (Figure 2), providing a special developmental context for understanding of tsRNA action.  
444 Here, we take a genome-wide, informatics-based approach toward establishing the mode of  
445 tsRNA action through the use of sponges for highly accumulated tsRNAs during this  
446 developmental transition. Our results suggest that tsRNAs can regulate gene expression  
447 through two distinct mechanisms acting on either mRNA levels or translation efficiency.  
448 tsRNAs accumulated in pupae exert preferential inhibitory effects on mRNA levels of genes  
449 involved in metamorphosis and on translation efficiency of genes encoding components of the  
450 translation machinery. These results document that tsRNAs accumulated at a developmental  
451 time exert regulatory activities at that time, suggesting that accumulation and action of  
452 tsRNAs are an integral part of the regulatory network instructing developmental progression  
453 (Figure 6D).

454

455       tsRNAs biogenesis is an inseparable aspect of tRNA biology and our study provides a  
456 first comprehensive atlas of tsRNAs during the larva-to-pupa transition in *Drosophila*. Here  
457 we adopted the mim-tRNAseq method to simultaneously quantitate tRNAs and tsRNAs,  
458 through the use of optimized size ranges in library construction and enzymatic treatments,  
459 primarily including T4PNK and TGIRT (Behrens et al. 2021). The length distribution of  
460 tsRNAs in our mim-tRNA/tsRNA-seq libraries peaks around 34 nt, which is generally  
461 consistent with a previous report using PANDORA-seq and small RNA-seq (Isakova et al.  
462 2020; Shi et al. 2021). This suggests that our approach provides a more reliable detection of  
463 tsRNAs than approaches using miRNA libraries. The clear demarcation detected at the  
464 anticodon loop and an inferred active processing of tRNAs into tsRNAs stem from our  
465 method that was tailored specifically for tsRNAs. As shown in the quantification results of  
466 different tsRNA subclasses (Figures 2E and S3C), mim-tRNA/tsRNA-seq exhibited an  
467 advantage in precisely detecting the 5'-tsRNA accumulation in early pupae. Such  
468 accumulation was further verified by Northern blots in the cases of 5'-tsRNA<sup>GlyGCC</sup>,  
469 5'-tsRNA<sup>GluCUC</sup> and 5'-tsRNA<sup>AspGUC</sup>. However, unlike the significant increase in 5'-tsRNA  
470 levels during the larva-to-pupa transition, tRNA levels appeared to be relatively stable. In  
471 addition, our analysis of TGIRT-introduced misincorporation identified little difference in  
472 tRNA modification profiles between larvae and early pupae (Supplemental Fig. S11).  
473 Because accumulation of 5'-tsRNAs takes place without significant changes in tRNA  
474 modifications analyzed, potential differences across developmental stages influencing such an  
475 accumulation likely come from other means, such as undetected modifications, the activity of

476 tRNA cleavage enzymes, or the stability of tsRNAs. A prominent contribution of 5-tRHs to  
477 the tsRNA accumulation (Figure 2G) supports a role of post-cleavage stability of tsRNAs in  
478 regulating tRNA/tsRNA homeostasis during the larva-to-pupa transition.

479

480 We have taken an informatics approach—complemented by gene-based  
481 analyses—toward an understanding of tsRNA action and specificity in a developmental  
482 system. Here we use two algorithms, TargetScan and miRanda, to probe the mode of  
483 tsRNA-mRNA interaction that can best explain our mRNA-seq data in response to sponge  
484 perturbations. These software had been employed to predict the posttranscriptional  
485 regulation of specific tsRNAs on putative target genes in human and *Drosophila* cells (Luo et  
486 al. 2018; Chen et al. 2022; Tu et al. 2023). We note that the utilization of these software as a  
487 tool in our study is not meant to be evidence for a strictly miRNA-like or seed-dependent  
488 mode of target recognition. To the contrary, based the observed regulatory properties  
489 tsRNAs on predicted targets using these bioinformatics tools, our results suggest a reduced  
490 dependence on both selection of seed positions and site locations relative to miRNAs. This  
491 distinction may be reflective of the differences in size, abundance, modifications and  
492 associated Argonaute proteins between tsRNAs and miRNAs. In *Drosophila*, miRNAs,  
493 siRNAs and piRNAs execute posttranscriptional regulation by primarily binding to AGO1,  
494 AGO2 and AGO3/PIWI/AUB, respectively (Okamura et al. 2004; Tomari et al. 2007; Iwasaki  
495 et al. 2015). While AGO3/PIWI/AUB are predominantly expressed in germline cells and  
496 early embryos, both AGO1 and AGO2 are expressed throughout the life cycle. According to  
497 our Western blot analysis (Supplemental Fig. S12), AGO2 might be the only Argonaute

498 protein expressed at a relatively high level in P2 pupae. It is possible that the presence of  
499 different AGO proteins at different developmental stages may contribute to the non-canonical  
500 target recognition mode of early pupae-accumulated tsRNAs.

501

502 Several miRNAs, including *bantam* and *miR-14*, have been reported to influence the  
503 fitness during this developmental transition by specifically targeting and tuning key hormonal  
504 pathways (Varghese and Cohen 2007; Boulan et al. 2013). In our study, the pupal lethality  
505 phenotype caused by tsRNA sponges suggests that 5'-tsRNA<sup>ProUGG</sup> and 5'-tsRNA<sup>AspGUC</sup> are  
506 required for successful completion of metamorphosis. The timing of lethality coincides with  
507 that of 5'-tsRNA accumulation to reach their peak expression levels. As shown in Figures  
508 4C and 6B, these tsRNAs act on a wide range of genes by regulating either the mRNA level  
509 or translation efficiency. The metamorphosis defects caused by tsRNA sponges are likely  
510 due to dysregulation of a collection of genes including, but not limited to, *Arc1* and *FASN2*.  
511 Accordingly, our rescue experiments to document the specificity of sponge-induced  
512 phenotype were performed by overexpressing full-length tRNAs, an approach that has been  
513 successfully used previously (Kuscu et al. 2018). Through the use of gene-based analyses,  
514 we have verified such specificity in both reporter assays and in a tissue-specific manner with  
515 the use of *FASN2* as a molecular marker. In our experiments, not all tsRNA sponges could  
516 cause a phenotype and, additionally, the defects were moderate for *Tubulin-GAL4*-driven one  
517 copy of the sponge transgenes. These results suggest that, similar to what has been observed  
518 with miRNA sponges (Davis et al. 2006; Esau 2008; Fulga et al. 2015), tsRNA sponges need  
519 to be present at a sufficient level to exert inhibitory activities.

520

521       The sponge approach has been widely used in studying miRNA functions. We adopted  
522 this approach to facilitate our analysis of tsRNAs that exhibit a newly uncovered property of  
523 accumulation at the larva-to-pupa transition. While this approach has provided useful  
524 insights into the action of these tsRNAs in our study, there are limitations inherent to all  
525 sponge-related approaches, especially when used in the tsRNA study. In particular, the gold  
526 standard of verifying the specificity of the phenotype induced by a miRNA sponge is through  
527 editing the miRNA gene itself (Cohen 2009), but this is not feasible for tsRNA sponges. In  
528 evaluating miRNA sponge specificity, another test is to compare the phenotype and gene  
529 expression profiles not only between a sponge and its negative control, but also between the  
530 negative control and no treatment (Ebert and Sharp 2010b). We have taken a similar test in  
531 our study and our results showed that, just like the wild-type line, the negative control lines  
532 exhibited neither the observed phenotypes nor specific effects on tsRNA target genes (Figures  
533 3D-E and 5B). In our analysis, putative tsRNA target genes that had elevated mRNA levels  
534 in sponge lines did not show such an increase in either the wild-type line or in the negative  
535 control lines (Figure 3 and Supplemental Fig. S7). Furthermore, we used two algorithms,  
536 miRanda and miRNAsong (Barta et al. 2016), to examine the interactions between our tsRNA  
537 sponges and their corresponding tsRNAs. The miRanda calculation suggested a highly  
538 stable structure (MFE < -59 kCal/mol) for all the five sponge-tsRNA pairs in this study, but  
539 the interactions between the tsRNA sponges and all known *Drosophila melanogaster*  
540 miRNAs were much less stable (MFE > -17 kCal/mol). The miRNAsong calculation (MFE  
541 cutoff: -25 kCal/mol and seed type: canonical 7mer) predicted four potential off-target

542 miRNAs: miR-9378-5p, miR-4949-5p, miR-1003-5p and miR-966-5p, but they all had a  
543 negligible expression in early pupal stages (PANDORA-seq: no detection; miRNA-seq: 0~44  
544 RPM). With respect to the phenotypes detected in two of the sponge lines, we used  
545 full-length tRNA expression in a rescue experiment. Our results showed that  
546 pre-tRNA<sup>AspGUC</sup> had a rescue effect in the 5'-tsRNA<sup>AspGUC</sup> sponge line, but not in the  
547 5'-tsRNA<sup>ProUGG</sup> sponge line, a finding supportive of sponge specificity. However, this  
548 rescue remained only partial, which underscores the limitations of both the perturbation and  
549 rescue approaches available to us in studying tsRNA action. Taken together, our results  
550 described in this report are supportive of the utility and specificity of tsRNA sponges despite  
551 a current insufficiency to formally rule out unintended effects including off-targets.

552

553 While this study suggests a role of tsRNAs in regulating both mRNA levels and  
554 translation efficiency during pupation, our current understanding remains incomplete. For  
555 example, according to our model (Figure 6D), tsRNA target genes in the translation group are  
556 preferentially down-regulated through a translation-mediated mechanism, whereas those in  
557 the metamorphosis group are down-regulated at their mRNA levels. Although both  
558 mechanisms have been suggested for tsRNA-mediated regulation (Goodarzi et al. 2015;  
559 Huang et al. 2017; Luo et al. 2018), it remains elusive how tsRNAs select different sets of  
560 target genes and act on them via different mechanisms within a single developmental context.  
561 In addition, tsRNAs could regulate developmental programs in ways that are distinct from the  
562 RNAi-like mechanism (Chen et al. 2016; Sharma et al. 2016; Chen et al. 2021a). Given the  
563 above-mentioned caveats about the use of tsRNA sponge and tRNA overexpression in vivo, it

564 is possible that alternative or additional functioning modes of tsRNAs may be operative  
565 during the larva-to-pupa transition. For example, while the pupa-accumulated tsRNAs do  
566 not appear to have an impact on either the levels or the activities of full-length tRNAs  
567 (Supplemental Fig. S6), they could act as aptamers for other gene regulatory machineries  
568 possibly via interacting with different biomolecules (Chen and Zhou 2023).

569

570 It has been well documented that tsRNAs derived from cleavage at the anticodon loop  
571 are induced by serum starvation, UV, hypoxia and other stresses (Lee and Collins 2005;  
572 Yamasaki et al. 2009; Emara et al. 2010; Sobala and Hutvagner 2013; Luo et al. 2018).  
573 Pupation represents a developmental stage that has an ‘internally starved’ state with limited  
574 energy production. Thus, a decline in global translation during the larva-to-pupa transition  
575 as seen in Figure 6A is a direct and effective solution to a cost-benefit optimization problem  
576 due to the huge cost of amino acid synthesis and polypeptide assembly (Yamada et al. 2020).  
577 Such a decline is accompanied by tsRNA accumulation without an apparent tRNA level  
578 reduction (Supplemental Fig. S1). Therefore, the performance objective of tsRNA  
579 accumulation here is not to deplete genuine tRNAs but to confine gene regulatory activities in  
580 the specific developmental context. As in serum-deprived S2 cells (Luo et al. 2018),  
581 tsRNAs accumulated in pupae preferentially reduce the translation efficiency of mRNAs  
582 coding for translation-related genes, thus allowing normal translation of other genes on  
583 demand. These results thus suggest a two-pronged design of embedding tsRNAs in the gene  
584 regulatory network instructing metamorphosis: translation-mediated action to influence  
585 overall translation and regulation of mRNA levels of metamorphosis-related genes. These

586 mechanisms together confer an ability to pupa-accumulated 5'-tsRNAs in safeguarding the  
587 progression of metamorphosis.

588

## 589 **Materials and methods**

### 590 **Fly husbandry, stocks, transgenic strains and classification of pupal stages**

591 All flies were reared and crossed on standard corn medium at 25 °C and 60% humidity.  
592 *Drosophila* stocks used in this study include *w<sup>1118</sup>*, *Actin-GAL4*, *Tubulin-GAL4*,  
593 *Eyeless-GAL4*, *Elav-GAL4*, *GMR-GAL4*, *Hh-GAL4*, *Ptc-GAL4*, *Vg-GAL4*, *MHC-GAL4*,  
594 *Dilp2-GAL4*, *Cg-GAL4*, *Phm-GAL4*, *Desat1-GAL4*.E800 (BDSC 65405),  
595 UAS-RPL13A-FLAG (BDSC 83684), *Drosophila simulans* (DSSC 14021-0251.195) and  
596 *Drosophila yakuba* (DSSC 14021-0261.01).

597

598 For each tsRNA sponge (against 5'-tsRNA<sup>GlyGCC</sup>, 5'-tsRNA<sup>GluCUC</sup>, 5'-tsRNA<sup>AspGUC</sup>,  
599 5'-tsRNA<sup>ProUGG</sup> or 5'-tsRNA<sup>LysUUU</sup>), 10 repeats of the sequence that is reversely  
600 complementary to 5' half of the corresponding mature tRNA with 4-bp spacers (Supplemental  
601 Table S2) were incorporated into the multiple cloning site (XhoII/XbaII), 34 bp downstream  
602 to the stop codon of eGFP (Figure 3A). As a negative control for 5'-tsRNA<sup>Asp</sup> sponge, a  
603 scrambled version of the reversely complementary sequence was generated using GenScript  
604 (Supplemental Table S2). For expression of pre-tRNA<sup>AspGUC</sup>, the genomic fragment of  
605 *tRNA:Asp-GTC-1-6* (FBgn0051602), from the upstream 223 bp to the downstream 228 bp,  
606 was amplified (see Supplemental Table S4 for PCR primers) and then inserted into the  
607 XhoII/XbaII sites of pUAST-attB. All the transgenic strains were created by integrating the

608 pUAST-attB vector with the donor transgenes to cytological positions 25C6, 68A4 and 75B1  
609 via the *phiC31* system. Microinjection services were provided by *Drosophila* resource and  
610 Technology Platform, Center of Excellence in Molecular and Cellular Sciences.

611

612 The chronological age after pupation was determined as the hours since the white pupa  
613 completely stopped wriggling. After that, 0~24 h, 24~48 h, 48~72 h and >72 h were labeled  
614 as P1-P4, respectively. According to the morphological markers, the P1-P4 ages of our *w<sup>1118</sup>*  
615 and the other control strains roughly correspond to Bownes's developmental stages p1~p5,  
616 p5~p6, p7~p9 and p10-p15 (Bainbridge and Bownes 1981), respectively.

617

## 618 **S2 cell culture, transfection and luciferase reporter assays**

619 *Drosophila* S2 cells were cultured in Schneider's Insect Medium (Gibco) containing  
620 10% FBS and Mycoplasma Prevention Reagent (TransGen FM501) without CO<sub>2</sub> to reach 2~4  
621 × 10<sup>6</sup> cells/mL. Transfection was performed in ~5 × 10<sup>5</sup> cells per well using transfection  
622 reagent according to the manufacturer's instruction (JetPRIME).

623

624 We utilized Dual-Luciferase Reporter Assay System (Promega) by cloning 3 tandem  
625 repeats of an endogenous target site (a perfect 7mer match to the nucleotides 2~8 of 5'-tsRNA  
626 + upstream 15 bp + downstream 8 bp; Supplemental Table S5) into the multiple cloning site  
627 (XhoI/NotI) of psiCHECK-2. For 5'-tsRNA<sup>Glu</sup>, 5'-tsRNA<sup>Gly</sup> and 5'-tsRNA<sup>Pro</sup>, the target  
628 sites were placed in the 3' UTR of *Renilla*; for 5'-tsRNA<sup>Asp</sup>, the target sites were incorporated

629 before the stop codon of *Renilla*. To contrast with the endogenous target sites, the mutated  
630 sites were created by scrambling the 7-mer seed match (Supplemental Table S5).

631

632 To examine the tsRNA actions and specificity, we performed co-transfection to quantify  
633 the effects of overexpression and sponge of tsRNAs on *Renilla* expression. For  
634 overexpression, cells were bathed with synthetic single-stranded RNA mimics of each  
635 5'-tsRNA (Supplemental Table S3; Azenta) at a final concentration of 20 nM, along with the  
636 pAWH vector expressing the corresponding full-length tRNA (Supplemental Table S4).  
637 After transfection for 48 h, the luciferase activities of *Firefly* and *Renilla* were measured  
638 according to the manufacturer's instruction (Promega).

639

#### 640 **RNA isolation and qRT-PCR**

641 Total RNA was isolated from tissue samples or S2 cell culture using RNAiso Plus  
642 (Takara 9108), and the concentration was measured by NanoDrop. For tRNA qRT-PCR,  
643 before reverse transcription, RNAs were pretreated by rtStar™ tRF&tiRNA Pretreatment Kit  
644 (Arraystar AS-FS-005) to remove internal m<sup>1</sup>A, m<sup>1</sup>G, and m<sup>3</sup>C. Reverse transcription was  
645 performed using HiScript III 1<sup>st</sup> Strand cDNA Synthesis Kit (Vazyme R312-01).  
646 Quantitative PCR was performed using 2× Universal SYBR Green Fast qPCR Mix (ABclonal  
647 RK21203) and quantified using LineGene 9600plus (Bioer Technology). Data from tissue  
648 samples were all normalized to *rp49*; *Renilla* data from Dual-Luciferase Reporter Assay in S2  
649 cells were normalized to *Firefly*. All RT-PCR primers are listed in Supplemental Table S6.

650

651 **Northern blot analysis and total RNA staining**

652 Briefly, 7~10  $\mu\text{g}$  of total RNA was routinely run in 10 mL of 10% PAGE gel with 7 M  
653 urea at 130V for about 1 h. Then, for detection of total tRNAs, SYBR-Gold (Invitrogen  
654 S11494) staining was performed. For Northern blot analyses, RNA was transferred to Nylon  
655 membranes (Millipore INYC00010) for 1h with 0.5 $\times$  TBE, cross-linked (UVP Crosslinker  
656 CX-2000UV), and hybridized at 55 $^{\circ}\text{C}$  overnight with 5' Digoxigenin-labelled probes  
657 (Supplemental Table S7) in hybridization buffer with 5 $\times$  SSC, 1% SDS and 1 $\times$  Denhardt's  
658 reagent (Sangon Biotech B548209). After blocking in maleic acid buffer with 1% block  
659 reagent (Roche 11096176001) at room temperature for 1 h, the membrane was incubated in  
660 blocking buffer with 1:10000 anti-DIG-AP antibody (Roche 11093274910). The membrane  
661 was washed in maleic acid buffer with Tween 20 for 15 min twice, incubated with pH 9.5  
662 detection buffer, reacted with CDP-Star (Roche 12041677001) at 37  $^{\circ}\text{C}$  for 15 min, and then  
663 exposed. Imaging was done using Chemilluminescence Imaging System (Clix), and  
664 quantification was done using ImageJ.

665

666 **cDNA library construction for tRNAs and tsRNAs**

667 A synthetic mimic of *E. coli* tRNA<sup>LysUUU</sup> (sequence in Supplemental Table S3; Azenta)  
668 was added to the total RNAs as a spike-in at 0.06 pmol/ $\mu\text{g}$ . Then the RNA samples were  
669 analyzed on 15% TBE-Urea gels alongside Low Range ssRNA Ladder (NEB N0364), and the  
670 60~100 nt (tRNA fraction) and 20~40 nt (tsRNA fraction) bands were respectively excised  
671 (For PANDORA-seq in L3 samples, 15-35nt bands were excised).

672

673 For mim-tRNA/tsRNA-seq, RNAs from both fractions were treated with deacylation  
674 buffer (pH = 9.0) and T4 PNK (NEB M021) to generate terminal 3'-OH and 5'-P ends. The  
675 resolved RNAs were sequentially ligated with 3'-adaptor and 5'-adaptor by T4 RNA ligase 2  
676 truncated (NEB M0242) and T4 RNA ligase 1 (NEB M0204), respectively. Reverse  
677 transcription was performed with TGIRT-III (HaiGene D0310) in low salt buffer (50 mM  
678 Tris-HCl pH = 8.3, 75 mM KCl, 3 mM MgCl<sub>2</sub>) at 42 °C for 16 h. For PANDORA-seq (Shi  
679 et al. 2021), the tsRNA fraction was treated with tRF&tiRNA Pretreatment Kit (Arraystar  
680 AS-FS-005) to generate terminal 3'-OH and 5'-P ends and to remove internal m<sup>1</sup>A, m<sup>1</sup>G, and  
681 m<sup>3</sup>C. The resolved RNAs were sequentially ligated with 3' and 5'-adaptors, and then  
682 reverse-transcribed with SuperScript™ IV (Thermo Fisher Scientific 18090010).

683

684 All cDNAs were amplified by Phusion DNA Polymerase (NEB M0530) through 14 PCR  
685 cycles, and the products within correct size ranges were collected for sequencing (Illumina  
686 NovaSeq 6000 PE150 for mim-tRNA/tsRNA-seq and PANDORA-seq; Illumina NovaSeq  
687 6000 SE50 PANDORA-seq in L3 samples).

688

### 689 **Ribosome profiling, Ribo-seq, RiboTag-seq and mRNA-seq**

690 Ribosome profiling and Ribo-seq library construction for larvae and pupae were  
691 performed as previously described (Zhang et al. 2018). Oenocyte-specific RiboTag  
692 experiments were performed on P2 pupae of  
693 *Desat1-GAL4>UAS-RPL13A-FLAG,UAS-5'-tsRNA<sup>AspGUC</sup>-sponge* or  
694 *Desat1-GAL4>UAS-RPL13A-FLAG,UAS-scramble* as previously described (Huang et al.

695 2019). Anti-FLAG antibody (Proteintech 66008-4-Ig) was used. Library construction for  
696 mRNA-seq was performed by VAHTS Universal V8 RNA-seq Library Prep Kit for Illumina  
697 (Vazyme NR605) or Biopharmaceutical Public Service Platform. Sequencing was  
698 performed with PE150 chemistry on Illumina NovaSeq 6000.

699

#### 700 **Sequencing reads processing, alignment and quantification**

701 For mRNA-seq and RiboTag-seq, reads were mapped to the *Drosophila melanogaster*  
702 genome (FlyBase r6.36) using HISAT2 v2.2.1 (Kim et al. 2019), and then summarized using  
703 featureCounts v2.0.1 (Liao et al. 2014). Fragments per kilobase of exon per million mapped  
704 (FPKM) was then calculated to quantify each mRNA-coding gene. For the differential  
705 expression analysis, the count data were normalized and analyzed using DESeq2 (Love et al.  
706 2014).

707

708 For Ribo-seq, after clipping for the adaptor sequences using cutadapt v3.4 (Martin 2011),  
709 reads with a remaining size of 26~34 nt were kept, and then sequentially mapped to rRNAs,  
710 tRNAs and the transcript with the longest CDS for each protein-coding gene using Bowtie2  
711 v2.2.5 (Langmead and Salzberg 2012) with default parameters. Ribosome protected  
712 fragment (RPF) was measured as the counts of reads uniquely mapped to the CDS (excluding  
713 the first 5 and the last 5 codons) and then normalized to per million total CDS-mapped reads.  
714 Translation efficiency (TE) was calculated as RPF/FPKM. At the single-codon resolution  
715 (Supplemental Fig. S6C), for each RPF read with a length of 30~32 nt, we determined the  
716 codon that occupies a ribosomal A-site as the 15<sup>th</sup>~17<sup>th</sup> trinucleotides from the 5' end and in

717 the same frame of CDS. All the other reads (~50%) were discarded to ensure the accuracy.  
718 For the genes enriched with codons matching with tRNA<sup>AspGUC</sup> (Supplemental Fig. S6D) we  
719 selected 1,112 genes with the top density of codons GAC/U for 5'-tsRNA<sup>AspGUC</sup> and  
720 mRNA-seq detection in all examined libraries.

721

722 For PANDORA-seq, reads within 20~40nt were kept after clipping adaptors, and then  
723 mapped to tRNAs using Bowtie2 v2.2.5 with default parameters. For  
724 mim-tRNA/tsRNA-seq, reads were processed and analyzed using mim-tRNAseq v1.2  
725 (Behrens et al. 2021) with the default parameters for *Drosophila melanogaster*.

726

#### 727 **Differential expression analysis, functional annotation and time-series profile clustering**

728 DEGs were considered with a significant change when FDR-adjusted  $p$ -value  $< 0.05$  and  
729  $|\log_2(\text{foldchange})| > 1$  in a DESeq2 analysis. For functional annotation, AnnotationDbi and  
730 clusterProfiler (Yu et al. 2012) were used with  $p\text{valueCutoff} = 0.01$ ,  $q\text{valueCutoff} = 0.05$ .  
731 For time-series analyses, Mfuzz (Kumar and M 2007) was used to perform soft clustering on  
732 the dynamic profiles of DEGs.

733

#### 734 **Prediction of tsRNA target genes**

735 To predict the target genes of tsRNAs that were accumulated in early pupae, we obtained  
736 all possible 7-mers from the tsRNA reads of mim-tRNA/tsRNA-seq data at the P2 stage.  
737 These 7-mers comprised a total of 2,075 unique seeds, from which 104 highly abundant seeds  
738 (top 5%) were retrieved. Then, TargetScan 7.0 (Agarwal et al. 2015) was used to predict

739 antisense perfect match in mRNA transcripts for the 104 seeds, and phyloP (Pollard et al.  
740 2010) was used to compute the conservation score of each putative target site. The densities  
741 of conserved sites (FDR-adjusted phyloP score < 0.001) in the mRNA transcripts of each  
742 protein-coding gene were summarized. Finally, we retrieved a total of 1418 genes with high  
743 site density (top 15%) and reliable mRNA expression (DESeq2-calculated baseMean > 70),  
744 and considered them as the target genes of P2-stage tsRNAs. For the five 5'-tsRNAs and  
745 antisense-scramble tsRNA, whose regulatory activities were further experimentally evaluated,  
746 we used TargetScan7.0 predicted conserved sites (FDR-adjusted phyloP score < 0.05) and an  
747 additional criterion of minimum free energy < -30 kcal/mol for the local alignment computed  
748 with miRanda (Enright et al. 2003).

749

#### 750 **Free fatty acid profiling**

751 Lipids were extracted from 30 mg of frozen tissues using a modified version of the Bligh  
752 and Dyer's method as described previously (Song et al. 2020). For each experimental  
753 setting, four independent samples were prepared stored at 80 °C until further analysis.  
754 Lipidomic analyses were conducted at LipidALL Technologies using a Shimadzu Nexera  
755 20AD HPLCcoupled with Sciex QTRAP 6500 PLUS as reported previously (Lam et al. 2021).  
756 Individual lipid species were quantified by referencing to spiked internal standards. Free  
757 fatty acids were quantitated using d31-16:0 (Sigma Aldrich) and d8-20:4 (Cayman  
758 Chemicals).

759

#### 760 **Western blot analysis**

761 Whole larvae or pupae at L3, P1 and P2 stages were lysed in RIPA lysis buffer (FUDE,  
762 FD009) with PMSF (Beyotime; ST506) and PhosStop phosphatase inhibitor cocktail  
763 (Beyotime; P1045). Rabbit anti-AGO1 (Abcam ab5070; 1:1000), Rabbit anti-AGO2  
764 (Abcam ab5072; 1:1000), HRP-conjugated  $\beta$ -Tubulin Mouse mAb (ABclonal AC030; 1:5000)  
765 and anti-rabbit HRP-conjugated secondary antibodies (FUDE FDR007) were used.

766

### 767 **Statistical significance**

768 For each sample subjected to deep sequencing in this study, the number of biological  
769 replicates and the mapping statistics were summarized in Supplemental Table S1. For  
770 Northern blot, Western blot, RT-qPCR and luciferase reporter assay respectively, each setting  
771 had at least two independent sample preparations and experiments. All statistical tests used  
772 in this study have been indicated in the legends to the related figures.

773

### 774 **Data access**

775 All raw RNA-sequencing data generated in this study have been submitted to the NCBI  
776 BioProject database (<https://www.ncbi.nlm.nih.gov/bioproject/>) under accession number  
777 PRJNA957228. All custom scripts required to reproduce the work have been deposited to  
778 [https://github.com/junlingshi/tsRNA\\_Drosophila\\_metamorphosis/](https://github.com/junlingshi/tsRNA_Drosophila_metamorphosis/).

779

### 780 **Competing interest statement**

781 The authors declare no competing interests.

782

783 **Acknowledgements**

784 This study was supported in part by the National Key R&D Program of China  
785 (2018YFA0800102 and 2021YFC2700403) and the National Natural Science Foundation of  
786 China (31871249 and 31871452). We acknowledge support of Zhejiang University (ZJU)  
787 School of Medicine affiliated Women's Hospital and Children's Hospital. We thank Hai  
788 Huang, JianHua Huang, Qi Zhou and Xiaohang Yang of ZJU for fly strains.

789

790 **Author contributions**

791 J.S., J.M. and F.H. conceived the study and designed the experiments; J.S. and J.X.  
792 performed experiments and generated data; J.S. analyzed the data and generated all figures;  
793 J.M. and F.H. acquired funding; J.S., J.M. and F.H wrote the paper and all approved the  
794 paper.

795

796 **References**

- 797 Agarwal V, Bell GW, Nam JW, Bartel DP. 2015. Predicting effective microRNA target sites in  
798 mammalian mRNAs. *Elife* **4**.
- 799 Ashley J, Cordy B, Lucia D, Fradkin LG, Budnik V, Thomson T. 2018. Retrovirus-like Gag Protein  
800 Arc1 Binds RNA and Traffics across Synaptic Boutons. *Cell* **172**: 262-274 e211.
- 801 Bainbridge SP, Bownes M. 1981. Staging the metamorphosis of *Drosophila melanogaster*. *J Embryol*  
802 *Exp Morphol* **66**: 57-80.
- 803 Barta T, Peskova L, Hampl A. 2016. miRNAson: a web-based tool for generation and testing of  
804 miRNA sponge constructs in silico. *Sci Rep* **6**: 36625.
- 805 Behrens A, Rodschinka G, Nedialkova DD. 2021. High-resolution quantitative profiling of tRNA  
806 abundance and modification status in eukaryotes by mim-tRNAseq. *Mol Cell* **81**: 1802-1815  
807 e1807.
- 808 Billeter JC, Atallah J, Krupp JJ, Millar JG, Levine JD. 2009. Specialized cells tag sexual and species  
809 identity in *Drosophila melanogaster*. *Nature* **461**: 987-991.
- 810 Boulan L, Martin D, Milan M. 2013. bantam miRNA promotes systemic growth by connecting insulin  
811 signaling and ecdysone production. *Curr Biol* **23**: 473-478.
- 812 Buccitelli C, Selbach M. 2020. mRNAs, proteins and the emerging principles of gene expression

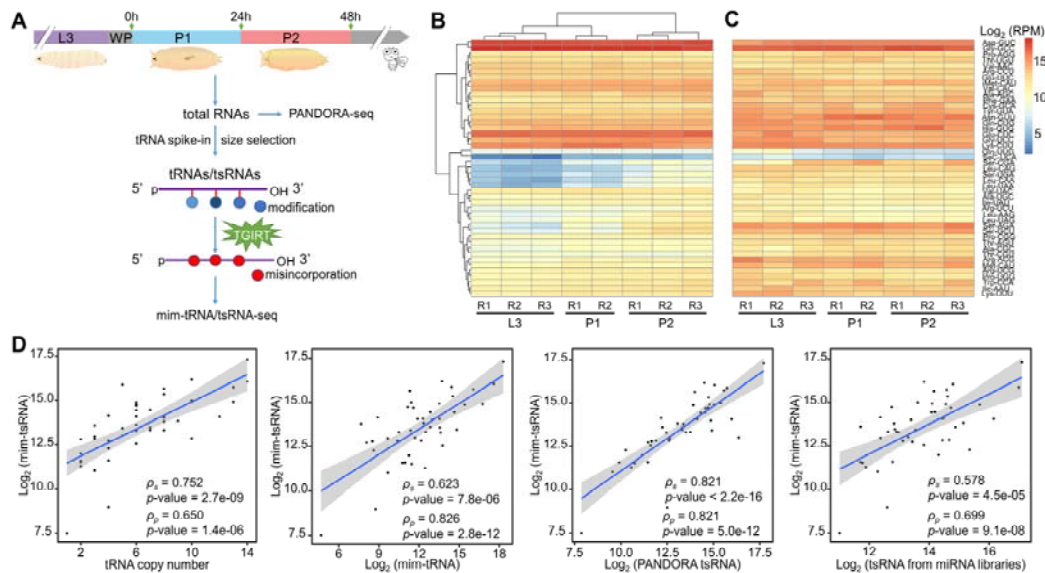
- 813 control. *Nat Rev Genet* **21**: 630-644.
- 814 Chen H, Xu Z, Cai H, Peng Y, Yang L, Wang Z. 2022. Identifying Differentially Expressed  
815 tRNA-Derived Small Fragments as a Biomarker for the Progression and Metastasis of  
816 Colorectal Cancer. *Dis Markers* **2022**: 2646173.
- 817 Chen L, Xu W, Liu K, Jiang Z, Han Y, Jin H, Zhang L, Shen W, Jia S, Sun Q et al. 2021a. 5' Half of  
818 specific tRNAs feeds back to promote corresponding tRNA gene transcription in vertebrate  
819 embryos. *Sci Adv* **7**: eabh0494.
- 820 Chen Q, Yan M, Cao Z, Li X, Zhang Y, Shi J, Feng GH, Peng H, Zhang X, Zhang Y et al. 2016. Sperm  
821 tsRNAs contribute to intergenerational inheritance of an acquired metabolic disorder. *Science*  
822 **351**: 397-400.
- 823 Chen Q, Zhang X, Shi J, Yan M, Zhou T. 2021b. Origins and evolving functionalities of tRNA-derived  
824 small RNAs. *Trends Biochem Sci* **46**: 790-804.
- 825 Chen Q, Zhou T. 2023. Emerging functional principles of tRNA-derived small RNAs and other  
826 regulatory small RNAs. *J Biol Chem* **299**: 105225.
- 827 Chung H, Loehlin DW, Dufour HD, Vaccarro K, Millar JG, Carroll SB. 2014. A single gene affects  
828 both ecological divergence and mate choice in *Drosophila*. *Science* **343**: 1148-1151.
- 829 Cohen SM. 2009. Use of microRNA sponges to explore tissue-specific microRNA functions in vivo.  
830 *Nat Methods* **6**: 873-874.
- 831 Couvillion MT, Bounova G, Purdom E, Speed TP, Collins K. 2012. A Tetrahymena Piwi bound to  
832 mature tRNA 3' fragments activates the exonuclease Xrn2 for RNA processing in the nucleus.  
833 *Mol Cell* **48**: 509-520.
- 834 Couvillion MT, Sachidanandam R, Collins K. 2010. A growth-essential Tetrahymena Piwi protein  
835 carries tRNA fragment cargo. *Genes Dev* **24**: 2742-2747.
- 836 Davis S, Lollo B, Freier S, Esau C. 2006. Improved targeting of miRNA with antisense  
837 oligonucleotides. *Nucleic Acids Res* **34**: 2294-2304.
- 838 Dou S, Wang Y, Lu J. 2019. Metazoan tsRNAs: Biogenesis, Evolution and Regulatory Functions.  
839 *Noncoding RNA* **5**.
- 840 Ebert MS, Neilson JR, Sharp PA. 2007. MicroRNA sponges: competitive inhibitors of small RNAs in  
841 mammalian cells. *Nat Methods* **4**: 721-726.
- 842 Ebert MS, Sharp PA. 2010a. Emerging roles for natural microRNA sponges. *Curr Biol* **20**: R858-861.
- 843 Ebert MS, Sharp PA. 2010b. MicroRNA sponges: progress and possibilities. *RNA* **16**: 2043-2050.
- 844 Emara MM, Ivanov P, Hickman T, Dawra N, Tisdale S, Kedersha N, Hu GF, Anderson P. 2010.  
845 Angiogenin-induced tRNA-derived stress-induced RNAs promote stress-induced stress  
846 granule assembly. *J Biol Chem* **285**: 10959-10968.
- 847 Enright AJ, John B, Gaul U, Tuschl T, Sander C, Marks DS. 2003. MicroRNA targets in *Drosophila*.  
848 *Genome Biol* **5**: R1.
- 849 Esau CC. 2008. Inhibition of microRNA with antisense oligonucleotides. *Methods* **44**: 55-60.
- 850 Fulga TA, McNeill EM, Binari R, Yelick J, Blanche A, Booker M, Steinkraus BR, Schnall-Levin M,  
851 Zhao Y, DeLuca T et al. 2015. A transgenic resource for conditional competitive inhibition of  
852 conserved *Drosophila* microRNAs. *Nat Commun* **6**: 7279.
- 853 Garrido D, Rubin T, Poidevin M, Maroni B, Le Rouzic A, Parvy JP, Montagne J. 2015. Fatty acid  
854 synthase cooperates with glyoxalase 1 to protect against sugar toxicity. *PLoS Genet* **11**:  
855 e1004995.
- 856 Gebetsberger J, Wyss L, Mleczko AM, Reuther J, Polacek N. 2017. A tRNA-derived fragment

- 857 competes with mRNA for ribosome binding and regulates translation during stress. *RNA Biol*  
858 **14**: 1364-1373.
- 859 Gebetsberger J, Zywicki M, Kunzi A, Polacek N. 2012. tRNA-derived fragments target the ribosome  
860 and function as regulatory non-coding RNA in *Haloferax volcanii*. *Archaea* **2012**: 260909.
- 861 Goodarzi H, Liu X, Nguyen HC, Zhang S, Fish L, Tavazoie SF. 2015. Endogenous tRNA-Derived  
862 Fragments Suppress Breast Cancer Progression via YBX1 Displacement. *Cell* **161**: 790-802.
- 863 Gramates LS, Agapite J, Attrill H, Calvi BR, Crosby MA, Dos Santos G, Goodman JL, Goutte-Gattat  
864 D, Jenkins VK, Kaufman T et al. 2022. FlyBase: a guided tour of highlighted features.  
865 *Genetics* **220**.
- 866 Guzzi N, Ciesla M, Ngoc PCT, Lang S, Arora S, Dimitriou M, Pimkova K, Sommarin MNE, Munita R,  
867 Lubas M et al. 2018. Pseudouridylation of tRNA-Derived Fragments Steers Translational  
868 Control in Stem Cells. *Cell* **173**: 1204-1216 e1226.
- 869 Haussecker D, Huang Y, Lau A, Parameswaran P, Fire AZ, Kay MA. 2010. Human tRNA-derived  
870 small RNAs in the global regulation of RNA silencing. *RNA* **16**: 673-695.
- 871 Huang B, Yang H, Cheng X, Wang D, Fu S, Shen W, Zhang Q, Zhang L, Xue Z, Li Y et al. 2017.  
872 tRF/miR-1280 Suppresses Stem Cell-like Cells and Metastasis in Colorectal Cancer. *Cancer*  
873 *Res* **77**: 3194-3206.
- 874 Huang K, Chen W, Zhu F, Li PW, Kapahi P, Bai H. 2019. RiboTag translomic profiling of  
875 *Drosophila* oenocytes under aging and induced oxidative stress. *BMC Genomics* **20**: 50.
- 876 Hussain S, Sajini AA, Blanco S, Dietmann S, Lombard P, Sugimoto Y, Paramor M, Gleeson JG, Odom  
877 DT, Ule J et al. 2013. NSun2-mediated cytosine-5 methylation of vault noncoding RNA  
878 determines its processing into regulatory small RNAs. *Cell Rep* **4**: 255-261.
- 879 Isakova A, Fehlmann T, Keller A, Quake SR. 2020. A mouse tissue atlas of small noncoding RNA.  
880 *Proc Natl Acad Sci U S A* **117**: 25634-25645.
- 881 Ivanov P, Emara MM, Villen J, Gygi SP, Anderson P. 2011. Angiogenin-induced tRNA fragments  
882 inhibit translation initiation. *Mol Cell* **43**: 613-623.
- 883 Iwasaki YW, Siomi MC, Siomi H. 2015. PIWI-Interacting RNA: Its Biogenesis and Functions. *Annu*  
884 *Rev Biochem* **84**: 405-433.
- 885 Keam SP, Sobala A, Ten Have S, Hutvagner G. 2017. tRNA-Derived RNA Fragments Associate with  
886 Human Multisynthetase Complex (MSC) and Modulate Ribosomal Protein Translation. *J*  
887 *Proteome Res* **16**: 413-420.
- 888 Kim D, Paggi JM, Park C, Bennett C, Salzberg SL. 2019. Graph-based genome alignment and  
889 genotyping with HISAT2 and HISAT-genotype. *Nat Biotechnol* **37**: 907-915.
- 890 Kim HK, Fuchs G, Wang S, Wei W, Zhang Y, Park H, Roy-Chaudhuri B, Li P, Xu J, Chu K et al. 2017.  
891 A transfer-RNA-derived small RNA regulates ribosome biogenesis. *Nature* **552**: 57-62.
- 892 Krishna S, Raghavan S, DasGupta R, Palakodeti D. 2021. tRNA-derived fragments (tRFs): establishing  
893 their turf in post-transcriptional gene regulation. *Cell Mol Life Sci* **78**: 2607-2619.
- 894 Kumar L, M EF. 2007. Mfuzz: a software package for soft clustering of microarray data.  
895 *Bioinformatics* **2**: 5-7.
- 896 Kumar P, Anaya J, Mudunuri SB, Dutta A. 2014. Meta-analysis of tRNA derived RNA fragments  
897 reveals that they are evolutionarily conserved and associate with AGO proteins to recognize  
898 specific RNA targets. *BMC Biol* **12**: 78.
- 899 Kumar P, Kuscuc C, Dutta A. 2016. Biogenesis and Function of Transfer RNA-Related Fragments  
900 (tRFs). *Trends Biochem Sci* **41**: 679-689.

- 901 Kuscus C, Kumar P, Kiran M, Su Z, Malik A, Dutta A. 2018. tRNA fragments (tRFs) guide Ago to  
902 regulate gene expression post-transcriptionally in a Dicer-independent manner. *RNA* **24**:  
903 1093-1105.
- 904 Lam SM, Zhang C, Wang Z, Ni Z, Zhang S, Yang S, Huang X, Mo L, Li J, Lee B et al. 2021. A  
905 multi-omics investigation of the composition and function of extracellular vesicles along the  
906 temporal trajectory of COVID-19. *Nat Metab* **3**: 909-922.
- 907 Langmead B, Salzberg SL. 2012. Fast gapped-read alignment with Bowtie 2. *Nat Methods* **9**: 357-359.
- 908 Lee SR, Collins K. 2005. Starvation-induced cleavage of the tRNA anticodon loop in *Tetrahymena*  
909 *thermophila*. *J Biol Chem* **280**: 42744-42749.
- 910 Li S, Xu Z, Sheng J. 2018. tRNA-Derived Small RNA: A Novel Regulatory Small Non-Coding RNA.  
911 *Genes (Basel)* **9**.
- 912 Li Y, Dong P, Yang Y, Guo T, Zhao Q, Miao D, Li H, Lu T, Xia F, Lyu J et al. 2022. Metabolic  
913 control of progenitor cell propagation during *Drosophila* tracheal remodeling. *Nat Commun* **13**:  
914 2817.
- 915 Liao Y, Smyth GK, Shi W. 2014. featureCounts: an efficient general purpose program for assigning  
916 sequence reads to genomic features. *Bioinformatics* **30**: 923-930.
- 917 Liu Y, Beyer A, Aebersold R. 2016. On the Dependency of Cellular Protein Levels on mRNA  
918 Abundance. *Cell* **165**: 535-550.
- 919 Lopez-Maury L, Marguerat S, Bahler J. 2008. Tuning gene expression to changing environments: from  
920 rapid responses to evolutionary adaptation. *Nat Rev Genet* **9**: 583-593.
- 921 Love MI, Huber W, Anders S. 2014. Moderated estimation of fold change and dispersion for RNA-seq  
922 data with DESeq2. *Genome Biol* **15**: 550.
- 923 Luo S, He F, Luo J, Dou S, Wang Y, Guo A, Lu J. 2018. *Drosophila* tsRNAs preferentially suppress  
924 general translation machinery via antisense pairing and participate in cellular starvation  
925 response. *Nucleic Acids Res* **46**: 5250-5268.
- 926 Martin M. 2011. Cutadapt removes adapter sequences from high-throughput sequencing reads. *EMBnet*  
927 *journal* **17**: 10-12.
- 928 Maute RL, Schneider C, Sumazin P, Holmes A, Califano A, Basso K, Dalla-Favera R. 2013.  
929 tRNA-derived microRNA modulates proliferation and the DNA damage response and is  
930 down-regulated in B cell lymphoma. *Proc Natl Acad Sci U S A* **110**: 1404-1409.
- 931 Merkey AB, Wong CK, Hoshizaki DK, Gibbs AG. 2011. Energetics of metamorphosis in *Drosophila*  
932 *melanogaster*. *J Insect Physiol* **57**: 1437-1445.
- 933 Mosher J, Zhang W, Blumhagen RZ, D'Alessandro A, Nemkov T, Hansen KC, Hesselberth JR, Reis T.  
934 2015. Coordination between *Drosophila* Arc1 and a specific population of brain neurons  
935 regulates organismal fat. *Dev Biol* **405**: 280-290.
- 936 Okamura K, Ishizuka A, Siomi H, Siomi MC. 2004. Distinct roles for Argonaute proteins in small  
937 RNA-directed RNA cleavage pathways. *Genes Dev* **18**: 1655-1666.
- 938 Pollard KS, Hubisz MJ, Rosenbloom KR, Siepel A. 2010. Detection of nonneutral substitution rates on  
939 mammalian phylogenies. *Genome Res* **20**: 110-121.
- 940 Rolff J, Johnston PR, Reynolds S. 2019. Complete metamorphosis of insects. *Philos Trans R Soc Lond*  
941 *B Biol Sci* **374**: 20190063.
- 942 Schaefer M, Pollex T, Hanna K, Tuorto F, Meusburger M, Helm M, Lyko F. 2010. RNA methylation  
943 by Dnmt2 protects transfer RNAs against stress-induced cleavage. *Genes Dev* **24**: 1590-1595.
- 944 Sharma U, Conine CC, Shea JM, Boskovic A, Derr AG, Bing XY, Belleannee C, Kucukural A, Serra

- 945 RW, Sun F et al. 2016. Biogenesis and function of tRNA fragments during sperm maturation  
946 and fertilization in mammals. *Science* **351**: 391-396.
- 947 Shi J, Zhang Y, Tan D, Zhang X, Yan M, Zhang Y, Franklin R, Shahbazi M, Mackinlay K, Liu S et al.  
948 2021. PANDORA-seq expands the repertoire of regulatory small RNAs by overcoming RNA  
949 modifications. *Nat Cell Biol* **23**: 424-436.
- 950 Sobala A, Hutvagner G. 2013. Small RNAs derived from the 5' end of tRNA can inhibit protein  
951 translation in human cells. *RNA Biol* **10**: 553-563.
- 952 Song JW, Lam SM, Fan X, Cao WJ, Wang SY, Tian H, Chua GH, Zhang C, Meng FP, Xu Z et al.  
953 2020. Omics-Driven Systems Interrogation of Metabolic Dysregulation in COVID-19  
954 Pathogenesis. *Cell Metab* **32**: 188-202 e185.
- 955 Su Z, Wilson B, Kumar P, Dutta A. 2020. Noncanonical Roles of tRNAs: tRNA Fragments and  
956 Beyond. *Annu Rev Genet* **54**: 47-69.
- 957 Tomari Y, Du T, Zamore PD. 2007. Sorting of Drosophila small silencing RNAs. *Cell* **130**: 299-308.
- 958 Tu M, Zuo Z, Chen C, Zhang X, Wang S, Chen C, Sun Y. 2023. Transfer RNA-derived small RNAs  
959 (tsRNAs) sequencing revealed a differential expression landscape of tsRNAs between  
960 glioblastoma and low-grade glioma. *Gene* **855**: 147114.
- 961 Tuorto F, Liebers R, Musch T, Schaefer M, Hofmann S, Kellner S, Frye M, Helm M, Stoecklin G,  
962 Lyko F. 2012. RNA cytosine methylation by Dnmt2 and NSun2 promotes tRNA stability and  
963 protein synthesis. *Nat Struct Mol Biol* **19**: 900-905.
- 964 Varghese J, Cohen SM. 2007. microRNA miR-14 acts to modulate a positive autoregulatory loop  
965 controlling steroid hormone signaling in Drosophila. *Genes Dev* **21**: 2277-2282.
- 966 Weigelt CM, Hahn O, Arlt K, Gruhn M, Jahn AJ, Esser J, Werner JA, Klein C, Buschges A, Gronke S  
967 et al. 2019. Loss of miR-210 leads to progressive retinal degeneration in Drosophila  
968 melanogaster. *Life Sci Alliance* **2**.
- 969 Yamada T, Hironaka KI, Habara O, Morishita Y, Nishimura T. 2020. A developmental checkpoint  
970 directs metabolic remodelling as a strategy against starvation in Drosophila. *Nat Metab* **2**:  
971 1096-1112.
- 972 Yamasaki S, Ivanov P, Hu GF, Anderson P. 2009. Angiogenin cleaves tRNA and promotes  
973 stress-induced translational repression. *J Cell Biol* **185**: 35-42.
- 974 Yu G, Wang LG, Han Y, He QY. 2012. clusterProfiler: an R package for comparing biological themes  
975 among gene clusters. *OMICS* **16**: 284-287.
- 976 Zhang H, Dou S, He F, Luo J, Wei L, Lu J. 2018. Genome-wide maps of ribosomal occupancy provide  
977 insights into adaptive evolution and regulatory roles of uORFs during Drosophila  
978 development. *PLoS Biol* **16**: e2003903.
- 979 Zhang L, Yang J, Li H, You J, Chatterjee N, Zhang X. 2020. Development of the transcriptome for a  
980 sediment ecotoxicological model species, *Chironomus dilutus*. *Chemosphere* **244**: 125541.

981



982

983

984

**Figure 1. Quantitative profiling of tRNA and tsRNA abundances during the larva-to-pupa transition of *Drosophila melanogaster***

985

(A) Experimental design to co-profile tRNAs and tsRNAs in 3<sup>rd</sup>-instar larvae (L3), 1<sup>st</sup> and 2<sup>nd</sup>-day pupae (P1 and P2).

986

987

(B-C) Heatmaps showing the abundances (RPM, reads per million mapped reads) of tRNAs and tsRNAs from whole-body extracts of the examined developmental stages, respectively.

988

989

Hierarchical clustering was performed on tRNA-seq libraries across different biological samples and across different tRNA genes (grouped according to the unique anticodons).

990

991

(D) Scatterplots show that at the same or close stage, tsRNA abundances were correlated with tRNA gene copy numbers, tRNA abundances, tsRNA abundances measured by

992

993

PANDORA-seq and tsRNA abundances measured by miRNA-seq (SRP048223 and SRP000602), respectively. Solid lines: linear regression models; shades: 95% confidence

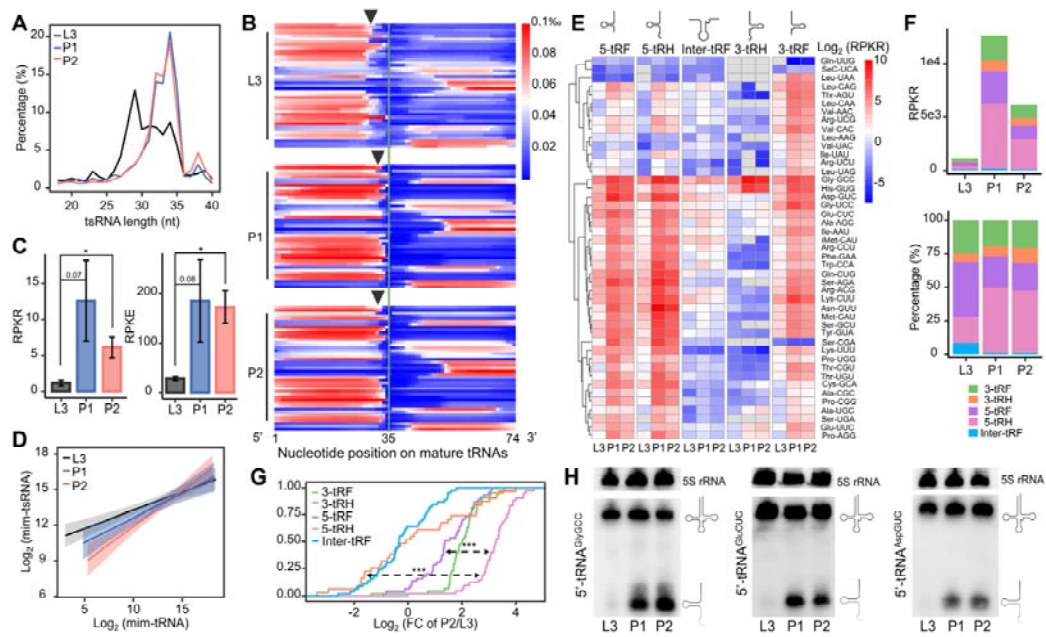
994

995

interval (CI). Pearson's correlation and Spearman's correlation were labeled as  $\rho_p$  and  $\rho_s$ ,

996

respectively.



997

998 **Figure 2. Expression level of 5'-tsRNAs increases during the larva-to-pupa transition**

999 (A) The length distributions of mim-tsRNA-seq reads in L3 (black), P1 (blue) and P2 (red).

1000 (B) A heatmap showing the normalized coverage of mim-tsRNA-seq reads at each nucleotide  
 1001 position along each mature tRNA. Each line presents one tRNA isoacceptor and they are  
 1002 ranked alphabetically. Note that the 3' ends of 5' tsRNAs in L3 are generally trimmed by ~2  
 1003 nt more than those in P1 and P2 (arrows marking the average positions of the 3' ends at each  
 1004 stage).

1005 (C) Quantifications of total tsRNAs of different developmental stages, performed using either  
 1006 2S rRNA as an internal control (RPKR, reads per kilo 2S rRNA reads) or *E. coli* tRNA<sup>LysUUU</sup>  
 1007 as a spike-in control (RPKE, reads per kilo *E. coli* tRNA reads). Error bars represent SEM  
 1008 (standard error of the mean) computed from two or three biological replicates. Asterisks  
 1009 indicate significant differences (Student's *t*-test  $p < 0.01$  denoted as \*\*).

1010 (D) Linear models of the relationships between tsRNA and tRNA abundances in L3 (black),  
 1011 P1 (blue) and P2 (red). The log-log slopes are 0.308, 0.416 and 0.604 for L3, P1 and P2,  
 1012 respectively.

1013 (E) A heatmap showing the tsRNA abundances (RPKR) in L3, P1 and P2 stages. The  
 1014 mim-tsRNA-seq reads mapped to all cytoplasmic tRNA genes were grouped into five

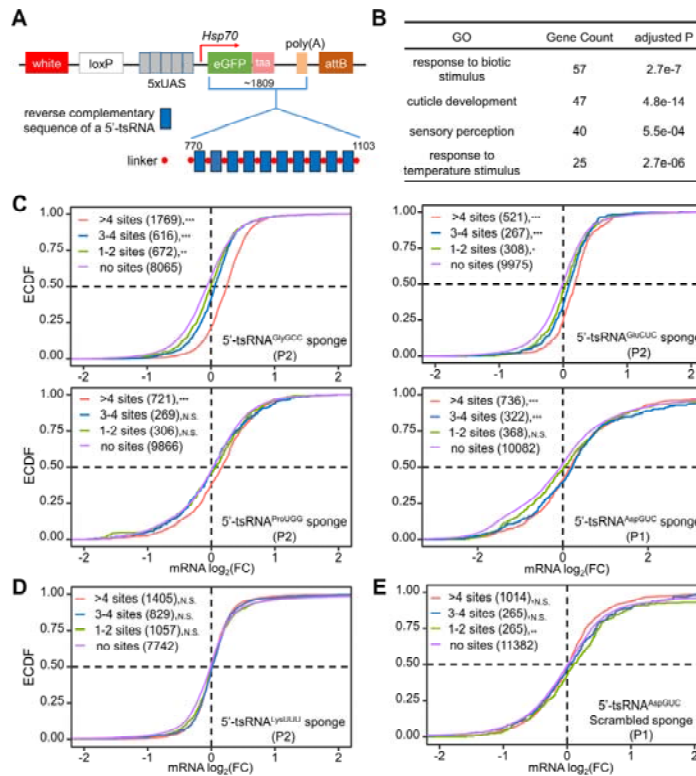
1015 subclasses: 5-tRF, 5-tRH, Inter-tRF, 3-tRH and 3-tRF.

1016 (F) Absolute (top) and relative (bottom) quantifications of total tsRNAs in each of the five  
1017 subclasses. 3-tRF (green), 3-tRH (orange), 5-tRF (purple), 5-tRH (pink) and Inter-tRF (blue).

1018 (G) Empirical Cumulative Distribution Function (ECDF) of the dynamic changes (P2/L3) in  
1019 tsRNA levels (measured as RPKR) of different subclasses. Kolmogorov–Smirnov tests  
1020 against the differences between 5-tRH vs 5-tRF and 5-tRH vs 3-tRH  $p < 0.001$  (\*\*\*) .

1021 (H) Northern blots using probes against the 5' ends of tRNA<sup>AspGUC</sup>, tRNA<sup>GlyGCC</sup> and  
1022 tRNA<sup>GluCUC</sup>. Each experiment has two independent replicates with consistent results.

1023



1024

1025

**Figure 3. Ubiquitous delivery of tsRNA sponges increases the levels of mRNAs with antisense target sites in early *Drosophila* pupae**

1026

1027

1028

1029

1030

1031

1032

1033

1034

1035

1036

1037

1038

1039

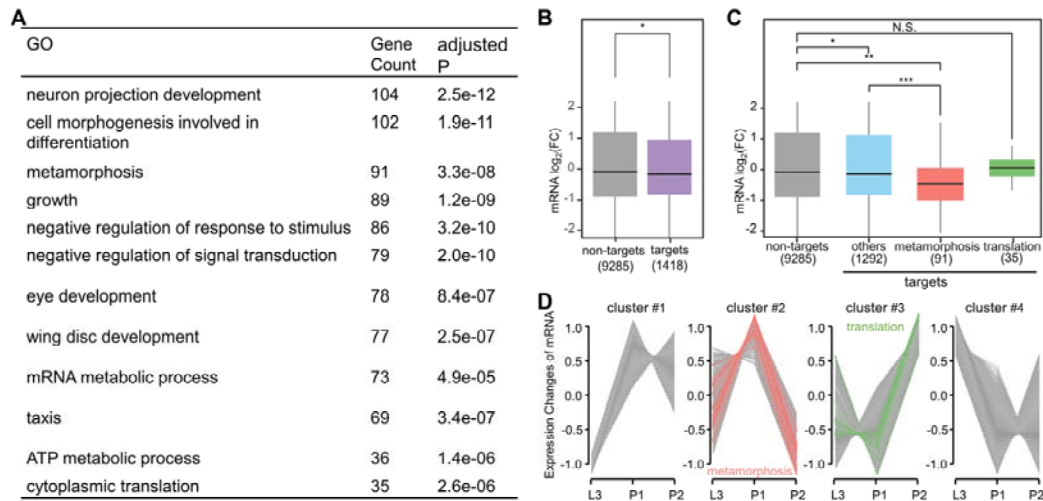
(A) Construction of tsRNA sponges. The sponge element consists of ten repetitive sequences (blue) that are complementary to a tsRNA of interest. It was placed within the 3' UTR of eGFP under the control of five UAS sites in an *attB* vector. Six sponge elements were generated against, respectively, 5'-tsRNA<sup>GlyGCC</sup>, 5'-tsRNA<sup>GluCUC</sup>, 5'-tsRNA<sup>ProUGG</sup>, 5'-tsRNA<sup>AspGUC</sup>, 5'-tsRNA<sup>LysUUU</sup> and a scrambled 5'-tsRNA<sup>AspGUC</sup> sequence. The expected sizes of the entire transcript and the sponge element for different tsRNA sponges are similar, and shown here are the numbers for 5'-tsRNA<sup>AspGUC</sup>. The transgenes were integrated into either attP40 (on 2<sup>nd</sup> chromosome) or attP2 (on 3<sup>rd</sup> chromosome) site via the *phiC31* system.

(B) Gene Ontology (GO) annotation reveals the enriched functional categories of 1,097 genes with significantly higher mRNA expression ( $\log_2(\text{fold change}) > 1$  and adjusted  $p < 0.05$ ) in the five *Tubulin*-GAL4-driven sponge lines than in *w<sup>1118</sup>*.

(C-E) ECDF plot of the fold differences in mRNA levels between each *Tubulin*-GAL4-driven sponge line and *w<sup>1118</sup>* (DESeq2-calculated baseMean > 50). For 5'-tsRNA<sup>GlyGCC</sup>,

1040 5'-tsRNA<sup>GluCUC</sup>, 5'-tsRNA<sup>ProUGG</sup>, 5'-tsRNA<sup>LysUUU</sup> (D) and their control, samples were  
1041 collected from P2 stage. For 5'-tsRNA<sup>AspGUC</sup> (C), the 5'-tsRNA<sup>AspGUC</sup> scramble (E) and their  
1042 control, samples were collected from P1 stage. Purple: genes without any predicted target  
1043 sites; green: genes with 1~2 sites; blue: genes with 3~4 sites; red: genes with >4 sites.

1044



1045

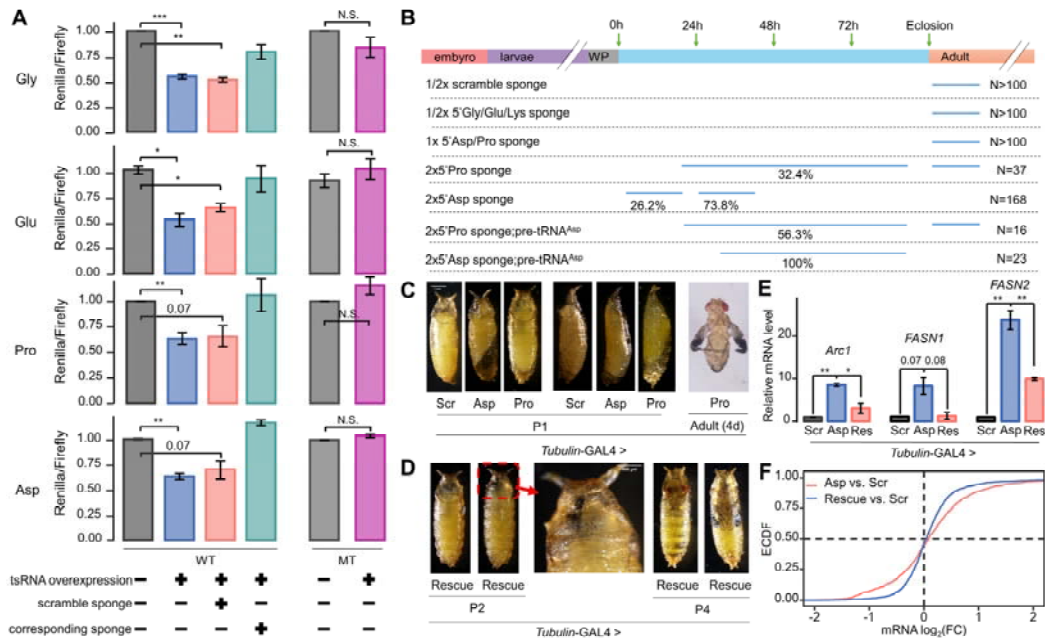
1046 **Figure 4. Identification of tsRNA function in early pupae**

1047 (A) GO enrichment of putative target genes (N = 1,418) of highly-expressed tsRNAs at P2  
1048 stage.

1049 (B) Shown are the fold differences between P2 and L3 in mRNA levels of putative tsRNA  
1050 target genes and non-target genes. Student's *t*-test  $p = 0.04$ .

1051 (C) Shown are the fold differences between P2 and L3 in mRNA levels of putative tsRNA  
1052 target genes in three functional categories: GO: 0007552 ('metamorphosis'), GO: 0002181  
1053 ('translation') and all other target genes ('others').

1054 (D) Clustering of the time-series mRNA expression profiles from L3 to P2. A total of 6,713  
1055 DEGs either between L3 and P1 or between P1 and P2 were used in the analysis.  
1056 Hypergeometric test  $p = 10^{-8}$  and  $10^{-7}$ , for the metamorphosis group enrichment in cluster #2  
1057 (red) and the translation group enrichment in cluster #3 (green), respectively.



1058

1059 **Figure 5. Evaluation of regulatory activities of 5'-tsRNAs in vitro and during**  
 1060 **development**

1061 (A) Normalized *Renilla/Firefly* reporter activities to assay target site-dependent regulation by  
 1062 5'-tsRNAs. WT: *Renilla* reporter gene carrying three target sites of each tsRNA. The  
 1063 sequences were cloned from native genes carrying predicted target sites (Supplemental Fig.  
 1064 S9B). MT: *Renilla* reporter gene carrying three sites with scrambled sequences in the seed  
 1065 match. For 5'-tsRNA<sup>GlyGCC</sup>, 5'-tsRNA<sup>GluCUC</sup> and 5'-tsRNA<sup>ProUGG</sup>, the sites were placed in 3'  
 1066 UTR; for 5'-tsRNA<sup>AspGUC</sup>, the sites were placed in CDS with the consideration of their higher  
 1067 inhibitory effects (Supplemental Fig. S7C). tsRNA overexpression: synthetic tsRNA mimic  
 1068 and the pAWH vector to express the corresponding pre-tRNA. tsRNA sponge: synthetic  
 1069 RNA sequence that is reversely complementary to the tsRNA. Scramble sponge: synthetic  
 1070 RNA sequence that is randomly scrambled from the sponge. See Supplemental Tables  
 1071 S2-S5 for the sequences.

1072 (B) Summary of the estimated lethality time based on the stage at which pupae stopped  
 1073 developing. For 5'-tsRNA<sup>GlyGCC</sup>, 5'-tsRNA<sup>GluCUC</sup>, 5'-tsRNA<sup>LysUUU</sup> and the scramble  
 1074 5'-tsRNA<sup>AspGUC</sup>, *Tubulin-GAL4*-driven one or two copies of sponge elements did not show  
 1075 any observable phenotypes (N > 100). For *Tubulin-GAL4*-driven one copy of sponge

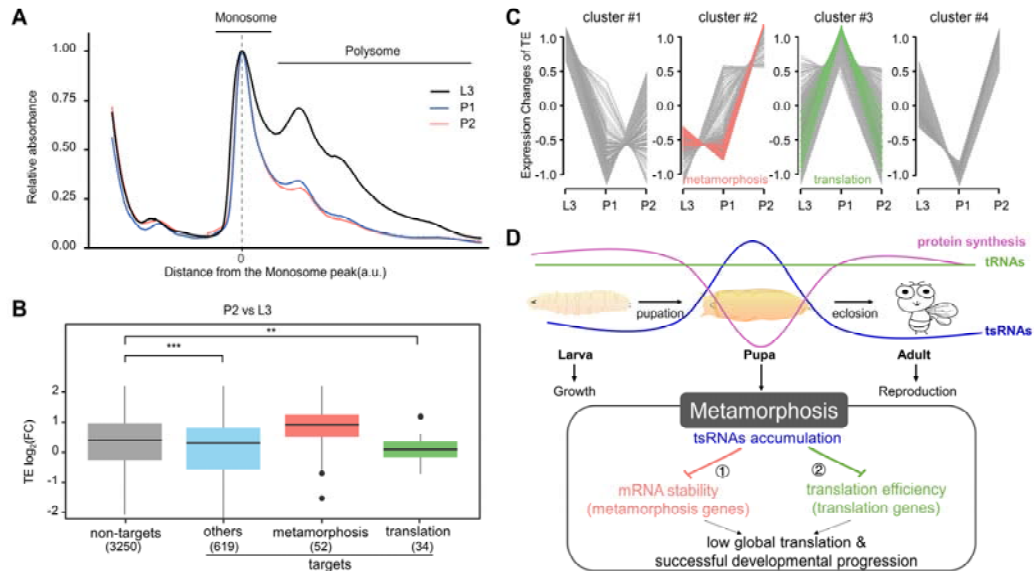
1076 element against 5'-tsRNA<sup>AspGUC</sup> and 5'-tsRNA<sup>ProUGG</sup>, some mild traits were observed but all  
1077 pupae emerged (N > 100).

1078 (C) The pupal lethality phenotype of *Tubulin*-GAL4-driven two copies of sponge elements  
1079 against 5'-tsRNA<sup>AspGUC</sup> and 5'-tsRNA<sup>ProUGG</sup>. All 5'-tsRNA<sup>AspGUC</sup>-sponge pupae ('Asp'; N =  
1080 168) did not survive beyond P2. 26.2% of them had an abnormal body curvature and died  
1081 during P1. 73.8% exhibited a failure in head inversion and an improper air bubble location  
1082 during P2. The 5'-tsRNA<sup>ProUGG</sup>-sponge pupae ('Pro'; N =37) showed high phenotypic  
1083 heterogeneity. 32.4% of them proceeded through P1 but failed to eclose. 67.6% emerged  
1084 with various defects such as un-spread wings 4 days after emergence. The *Tubulin*-GAL4  
1085 driven two copies of scramble sponge ('Scr') was used as control, and all tested pupae (N >  
1086 100) emerged without observable defects.

1087 (D) Phenotypic rescue with pre-tRNA<sup>AspGUC</sup>. All rescued pupae ('Rescue'; N = 23)  
1088 proceeded through P1 with finished head evert process and correct air bubble location.  
1089 43.5% of them lived to P4 as late pharate adults, but had leg malformation and did not eclose.

1090 (E) qRT-PCR confirming that the mRNA levels of three selected 5'-tsRNA<sup>AspGUC</sup> target genes  
1091 were restored by pre-tRNA<sup>AspGUC</sup>. All samples were collected from P1 pupae. *Arc1*,  
1092 *FASN1* and *FASN2* were selected due to their known expression and function during the  
1093 larva-to-pupa transition. *rp49* was used as internal control. Each experiment had two  
1094 independent replicates. Errorbars represent SEM, and Student's *t*-tests were used.

1095 (F) mRNA-seq confirming that the mRNA levels of 5'-tsRNA<sup>AspGUC</sup> target genes (N = 1,411)  
1096 were restored by pre-tRNA<sup>AspGUC</sup>. Kolmogorov–Smirnov test *p*-value = 10<sup>-11</sup>.



1097

1098 **Figure 6. Translation genes that are targeted by pupa-accumulated tsRNAs exhibit a**  
 1099 **reduction in translation efficiency during pupation**

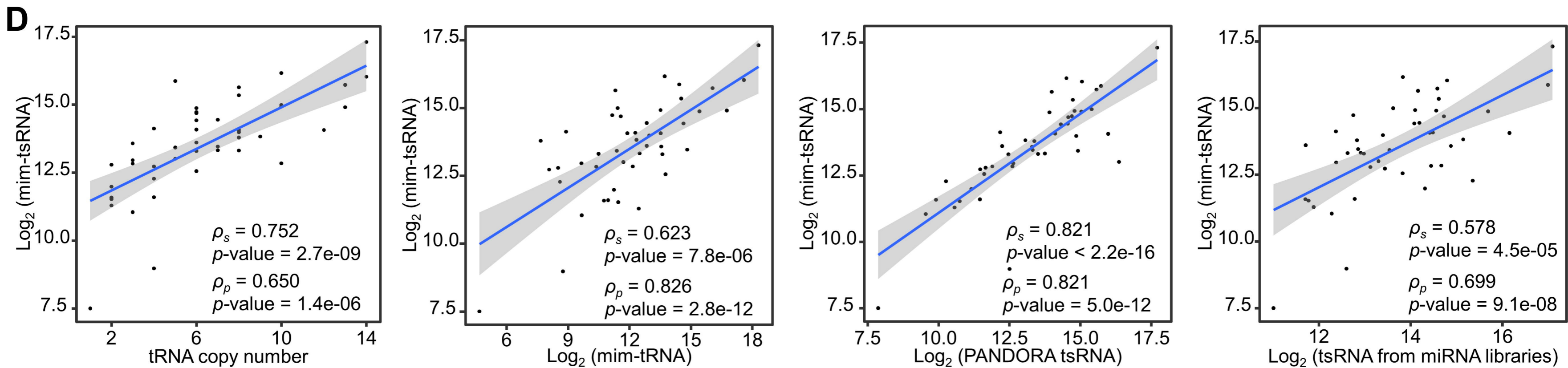
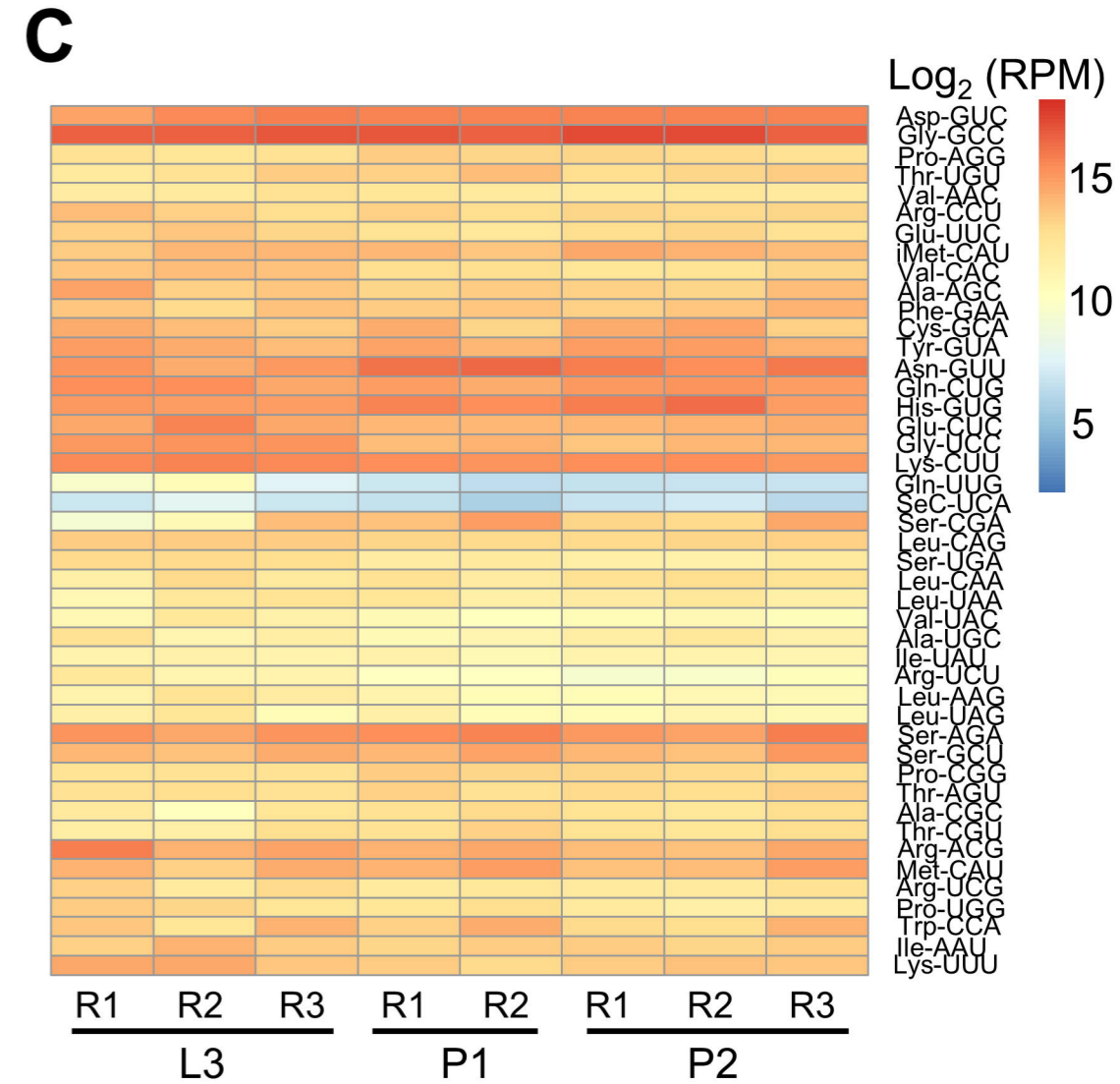
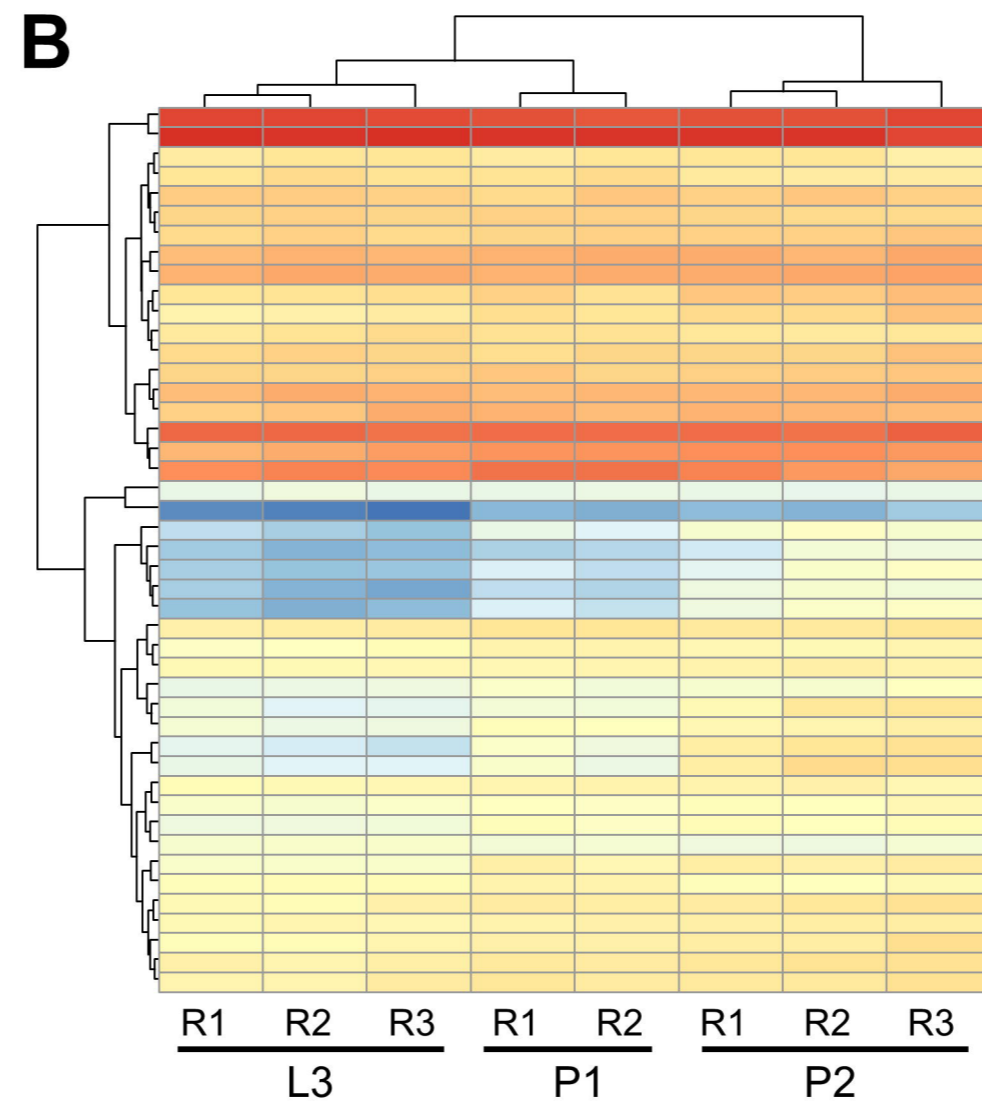
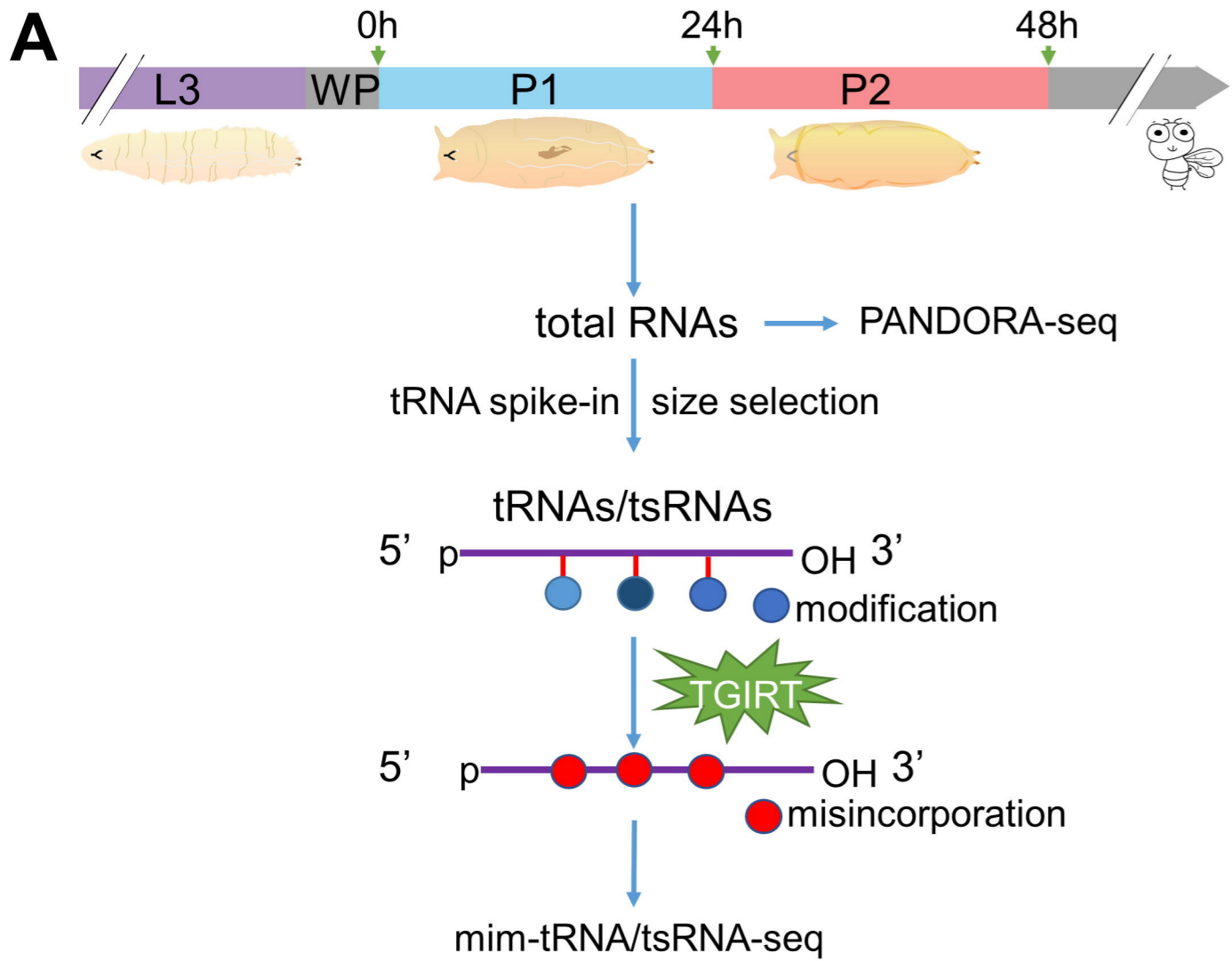
1100 (A) Absorbance profiles at 254 nm of RNA samples from L3 (gray), P1 (blue) and P2 (green).  
 1101 For each experiment, both the absorbance and the position were normalized to the 80S  
 1102 monosome peak.

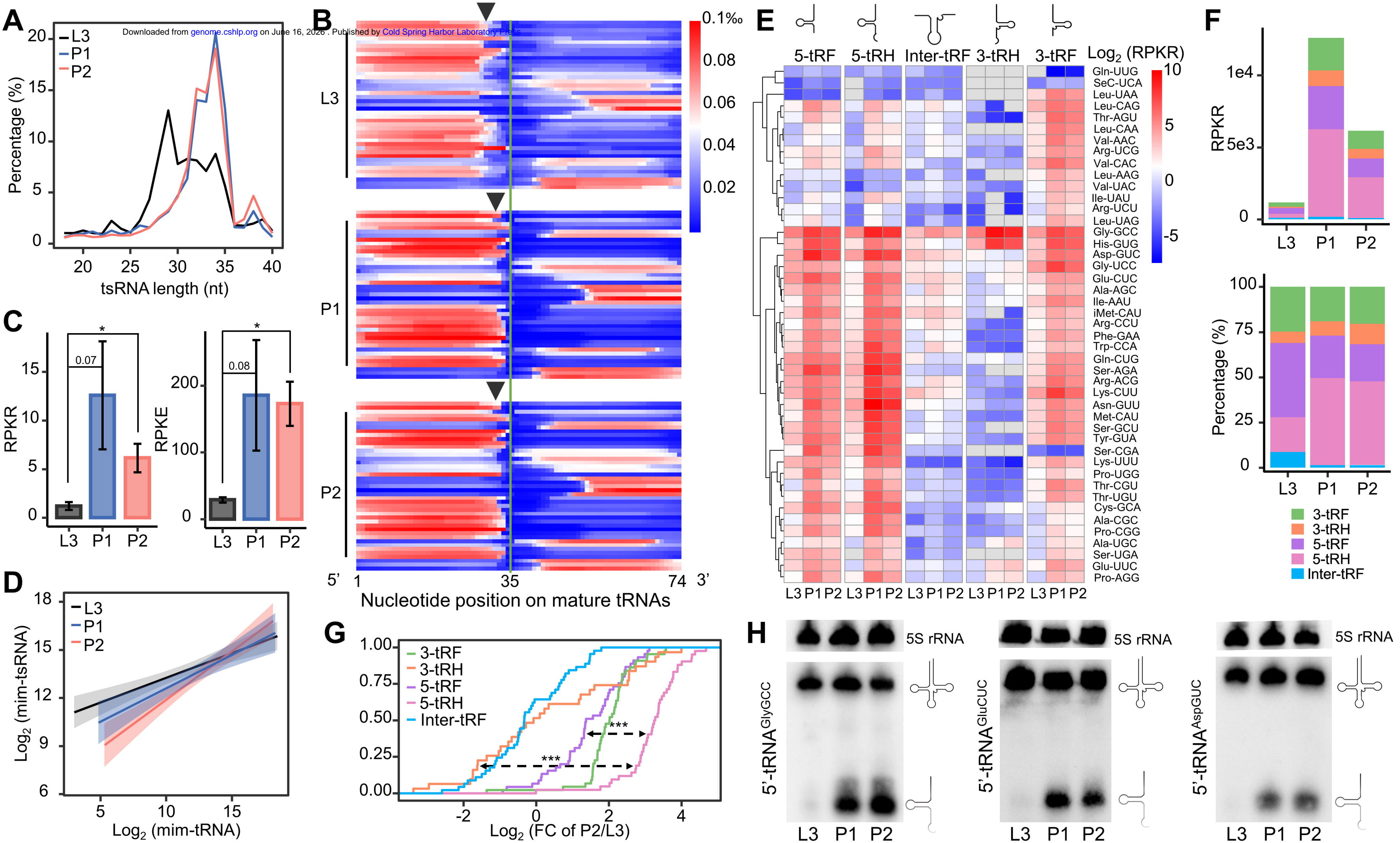
1103 (B) Shown are the fold differences between P2 and L3 in translation efficiency (TE) of  
 1104 putative tsRNA target genes in different functional categories. Protein-coding genes that  
 1105 had mRNA-seq FPKM > 10 in both L3 and P2 were included.

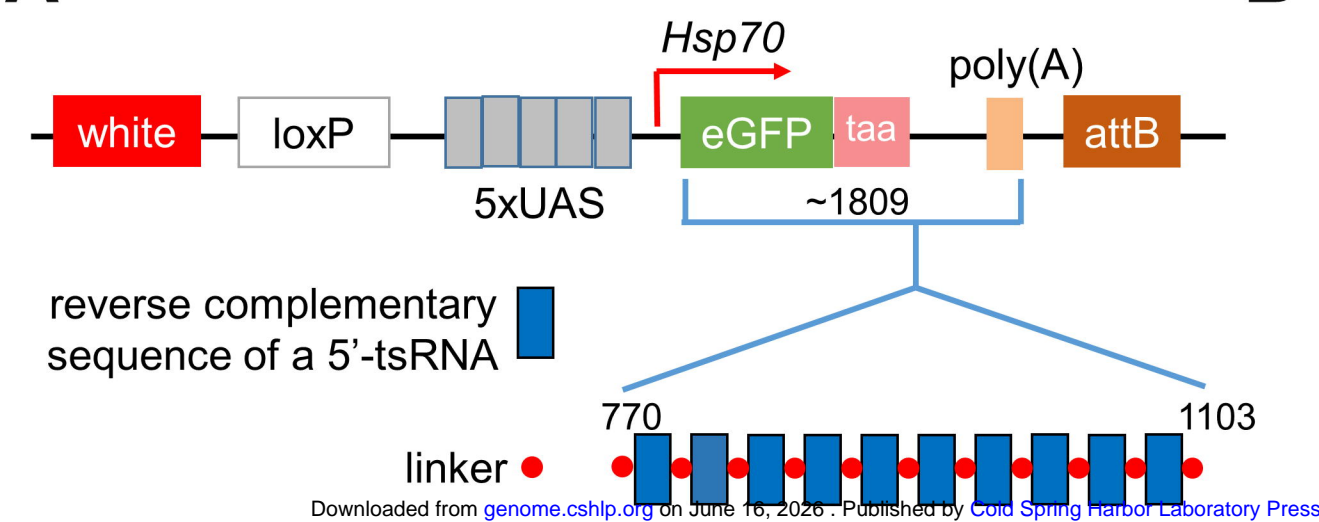
1106 (C) Clustering of the time-series TE profiles from L3 to P2. A total of 3,380 genes  
 1107 (mRNA-seq FPKM > 5) with TE that differed by at least twofold either between L3 and P1 or  
 1108 between P1 and P2 were used in the analysis. Hypergeometric test  $p = 10^{-4}$  and  $10^{-6}$ , for the  
 1109 metamorphosis group enrichment in cluster #2 (red) and the translation group enrichment in  
 1110 cluster #3 (green), respectively.

1111 (D) A graphic illustration of tsRNA regulatory activities during the larva-to-pupa transition of  
 1112 *Drosophila*. Despite the stable level of tRNAs (green), this transition is marked with an  
 1113 accumulation of tsRNAs (blue) and a decline of overall protein synthesis (purple), providing a  
 1114 special developmental context for understanding of tsRNA action. In a target site-dependent  
 1115 manner, the early pupa-accumulated tsRNAs specifically down-regulate gene expression in

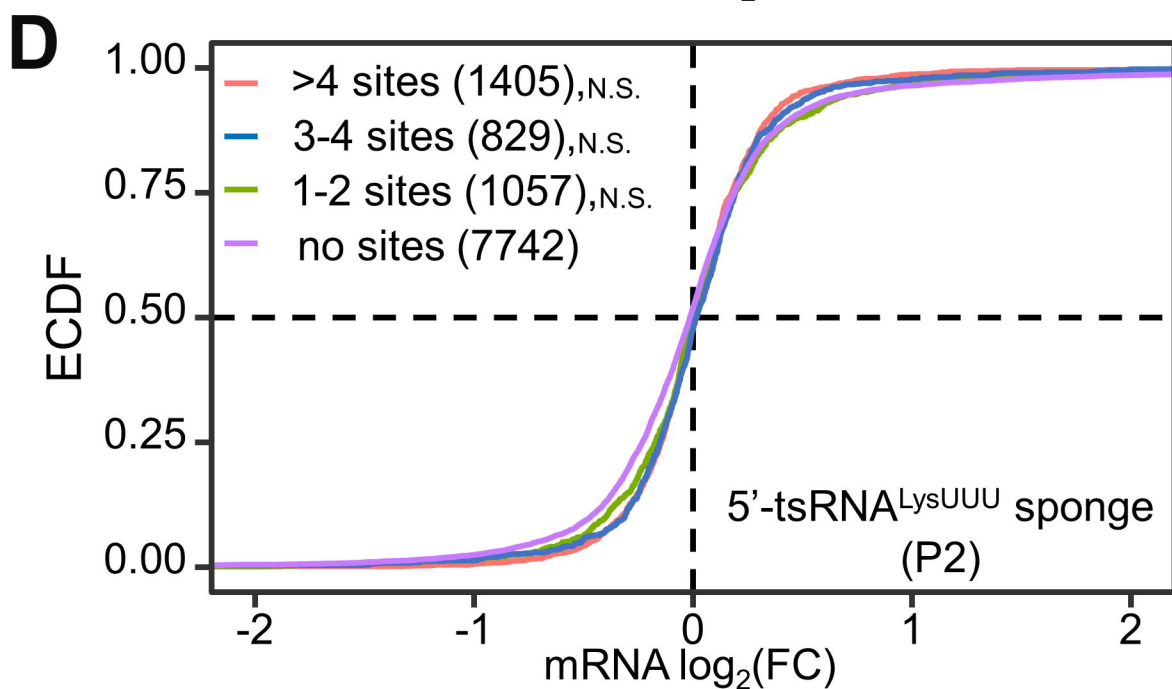
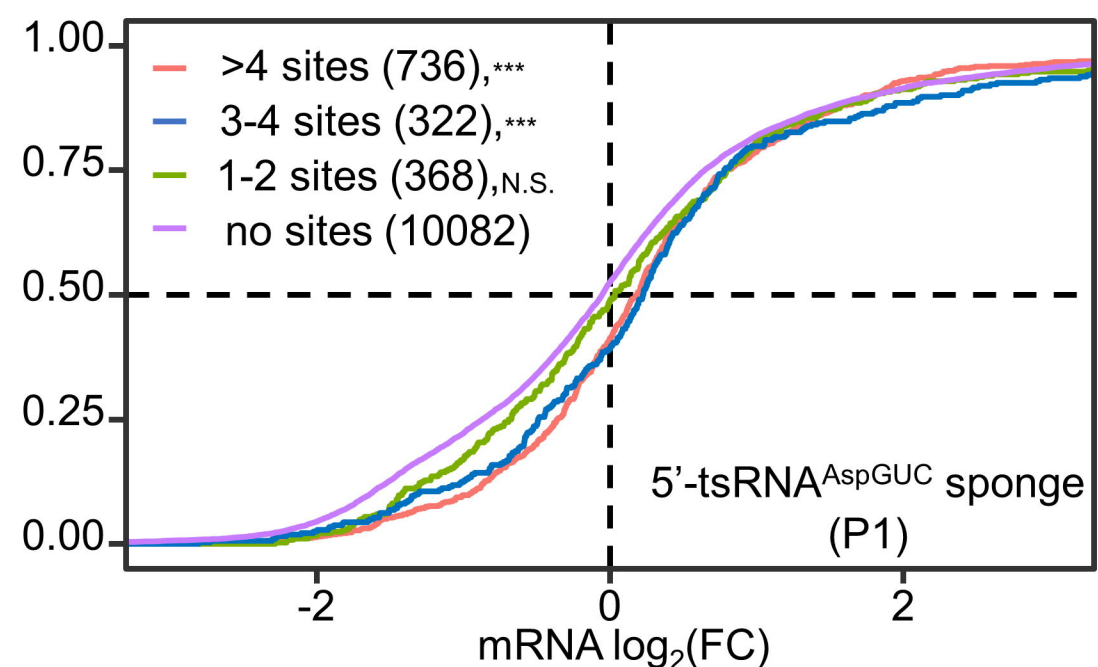
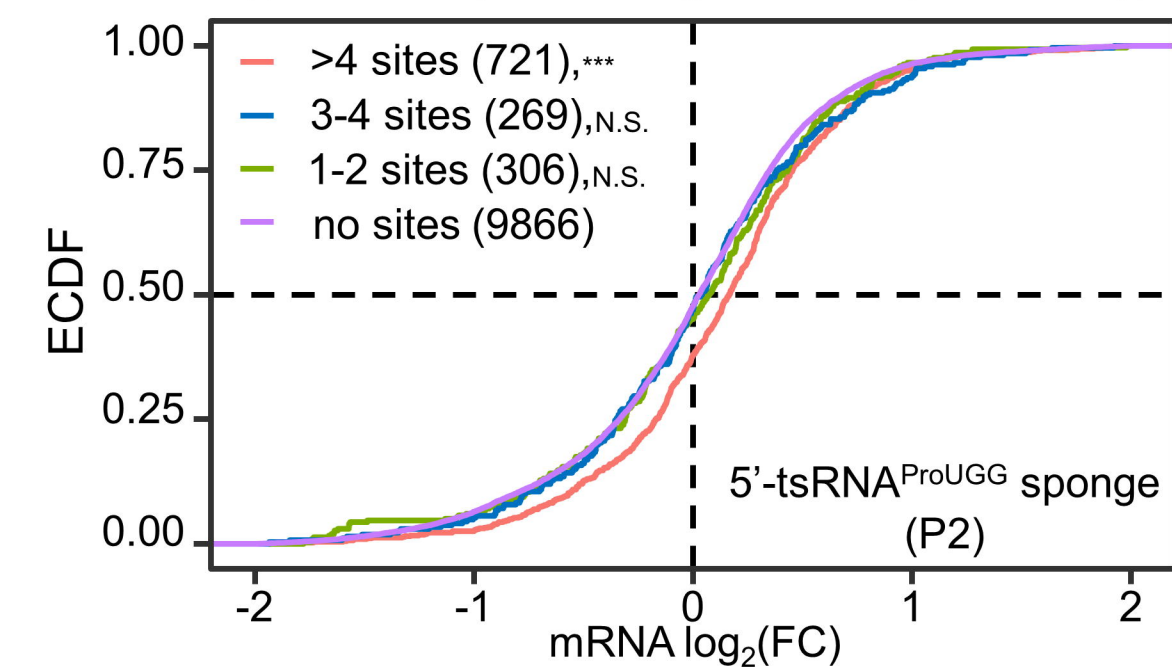
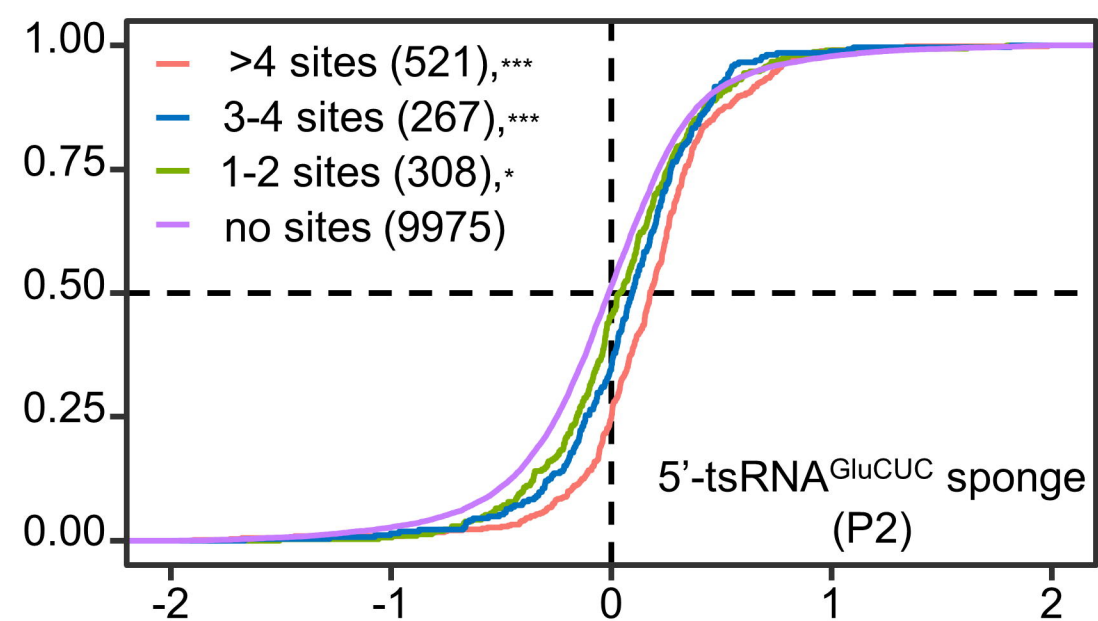
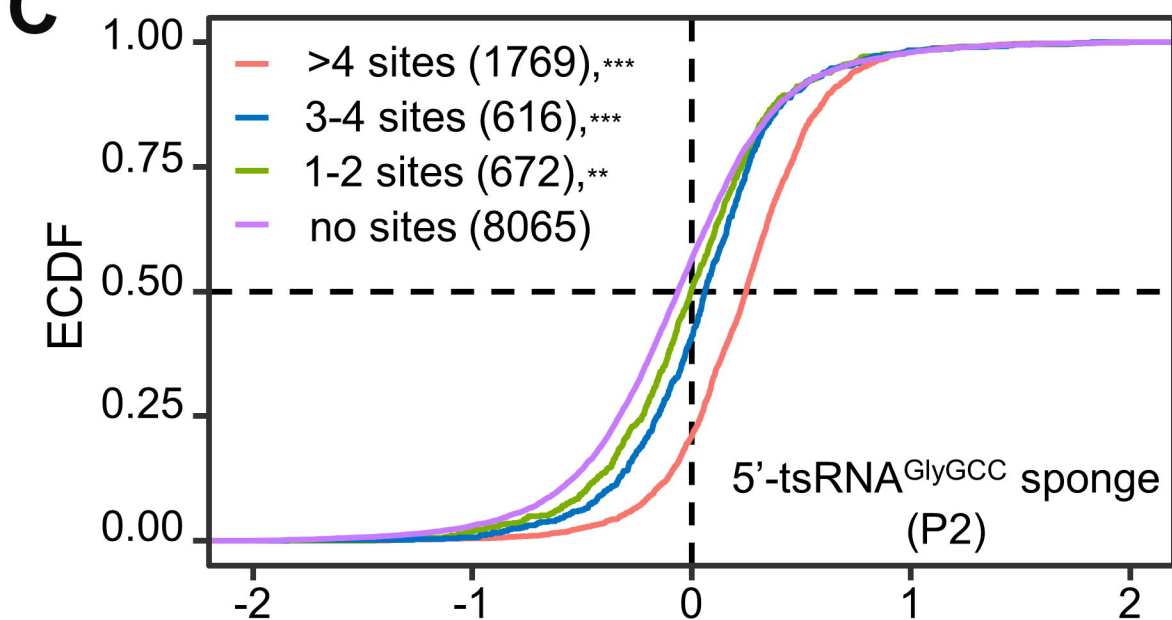
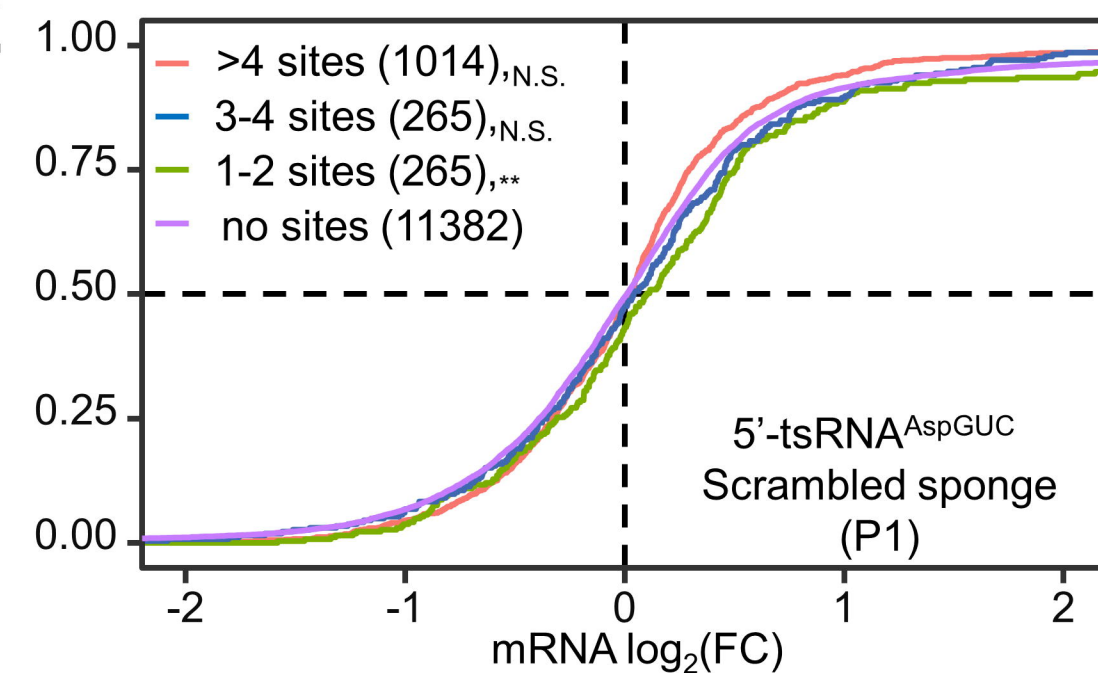
1116 the metamorphosis group at the mRNA level (suppression arrow 1) and genes in the  
1117 translation group at the translation level (suppression arrow 2). Subsequently, the global  
1118 translation activity is reduced. Under this framework, the accumulation of  
1119 functionally-active tsRNAs instruct *Drosophila* metamorphosis to proceed through the  
1120 larva-to-pupa-to-adult transition.





**A****B**

GO	Gene Count	adjusted P
response to biotic stimulus	57	2.7e-7
cuticle development	47	4.8e-14
sensory perception	40	5.5e-04
response to temperature stimulus	25	2.7e-06

**C****E**

**A**

GO	Gene Count	adjusted P
neuron projection development	104	2.5e-12
cell morphogenesis involved in differentiation	102	1.9e-11
metamorphosis	91	3.3e-08
growth	89	1.2e-09
negative regulation of response to stimulus	86	3.2e-10
negative regulation of signal transduction	79	2.0e-10
eye development	78	8.4e-07
wing disc development	77	2.5e-07
mRNA metabolic process	73	4.9e-05
taxis	69	3.4e-07
ATP metabolic process	36	1.4e-06
cytoplasmic translation	35	2.6e-06

